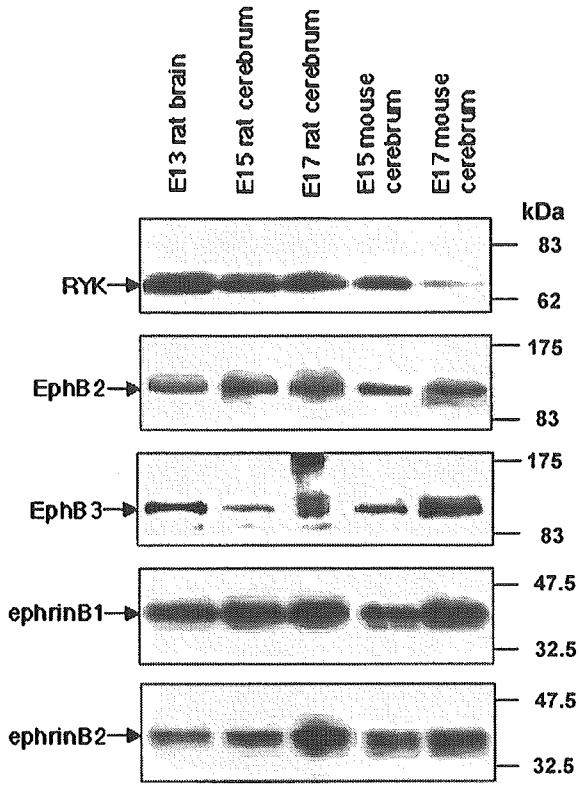

Fig. 1. Western blot analyses of RYK, EphB2/B3, and ephrinB1/B2. Extracts of brains were analyzed by the Western blot for each antibody. Arrows point to specifically detected signals. RYK, EphB2, EphB3, ephrinB1, and ephrinB2 are expressed in embryonic brain.

sion was detected in the brain of rat embryos, consistent with our previous findings obtained by in situ hybridization and immunohistochemistry [8,9]. RYK expression was also observed in embryonic mouse cerebrum. EphB2 and EphB3 were detected in the cerebrum of both rats and mice. Both ephrinB1 and ephrinB2 were detected in the embryonic cerebrum of rats and mice. No expression of ephrinB3 was detected in developing brain (data not shown), and this result was consistent with those of studies showing little expression of ephrinB3 in the anterior part of embryonic brain [32]. Overall, RYK, EphB2, EphB3, ephrinB1, and ephrinB2 are expressed in embryonic brain, suggesting possible interactions between RYK and Eph receptors during cortical development.

Binding of rat RYK to EphB3 in vitro

Previous in vitro analyses have shown that mouse and human RYK is capable of binding to EphB2 and EphB3 receptors [16,20]. To clarify the biochemical characteristics of rat RYK, COS-7 cells were transfected with FLAG-tagged rat RYK together with HA-tagged EphB3, and the cell lysate was immunoprecipitated and immunoblotted. FLAG-tagged RYK deletion mutants were also used for the same series of analyses (Fig. 2).

As shown in Fig. 3, signals for RYK, dTK, and dLRM in the COS-7 cell lysates were detected at

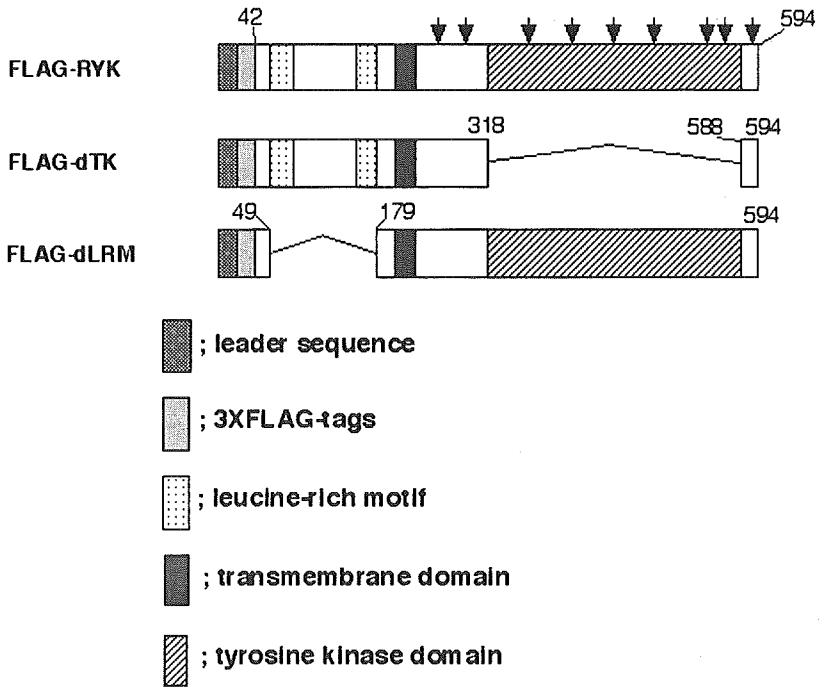

Fig. 2. Schematic diagrams of RYK and its deletion mutants. Deduced amino acid numbers of rat RYK (GenBank Accession No. AY669340) are indicated. dTK lacks the entire tyrosine kinase in the intracellular domain. dLRM lacks both leucine-rich motifs. Arrowheads indicate the locations of intracellular tyrosine residues.

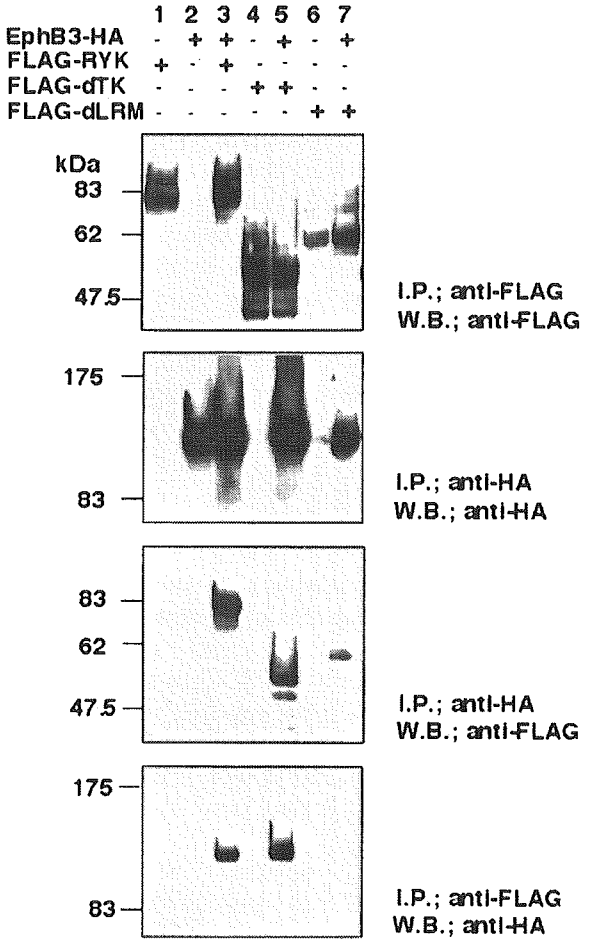

Fig. 3. Binding of RYK to EphB3 in vitro. Extracts of COS-7 cells, transfected with the plasmids indicated, were immunoprecipitated with anti-FLAG antibody or anti-HA antibody and immunoblotted with anti-FLAG antibody or anti-HA antibody. FLAG-RYK and FLAG-dTK precipitated with EphB3-HA (lanes 3 and 5, respectively), but much smaller amounts of FLAG-dLRM precipitated with EphB3-HA (lane 7). IP, immunoprecipitation; WB, Western blot.

around 75, 50, and 60 kDa, respectively. Their signals were larger than those deduced from the amino acid sequence, possibly because of glycosylation and insertion of FLAG tags. The signal for EphB3 was detected at around 120 kDa. Immunoprecipitation with anti-HA antibody followed by immunoblotting with anti-FLAG antibody revealed a high level of co-precipitation of RYK and EphB3. A similar level of co-precipitation of dTK and EphB3 was observed, but much less dLRM co-precipitated with EphB3. Immunoprecipitation with anti-FLAG antibody followed by immunoblotting with anti-HA antibody also revealed co-precipitation of EphB3 with RYK and dTK, but much less EphB3 was precipitated with dLRM. These observations suggested binding of rat RYK to EphB3 in vitro and that the LRMs in the extracellular domain of RYK are crucial to the binding between these molecules.

Overexpression of RYK in cortical slice cultures suppressed cell migration

Our previous studies have shown expression of RYK in neuronal progenitor cells in the ventricular zone and mature neurons in the cortical plate [8,9]. Independently, the Eph signaling pathway has been implicated in the migration of neurons in developing cortex [28]. These findings, together with the in vitro binding of RYK and the Eph receptor, support the hypothesis that RYK plays an important role in cell migration during cortical development, and cell migration was analyzed in embryonic cortical slice cultures after overexpression of EGFP-fused RYK and its mutants in ventricular zone cells to test this hypothesis (Fig. 4).

At 24 h after electroporation, most cells transfected with each plasmid were observed in the ventricular zone or subventricular zone. RYK-EGFP, dTK-EGFP, and dLRM-EGFP largely localized in the cell membrane, while EGFP broadly distributed in the cytoplasm. Some transfected cells were bipolar, with leading processes oriented radially to the pial surface, exhibiting the morphology of migrating neurons [31,33]. At 48 h after the electroporation, EGFP-expressing cells were broadly distributed between the ventricular surface and the intermediate zone, whereas most RYK-EGFP-expressing cells remained in the ventricular or subventricular zone. At this stage, some dLRM-EGFP-expressing cells had already migrated to the intermediate zone the same as EGFP-expressing cells, whereas a large number of dTK-EGFP-expressing cells had hardly migrated toward the cortical plate at all. At 72 h after electroporation, cells expressing EGFP and dLRM-EGFP were widely distributed, and some of them had already migrated to the cortical plate. By contrast, hardly any RYK-EGFP- and dTK-EGFP-expressing cells had migrated extensively, and almost all of them remained in the ventricular or subventricular zone. At this stage, a number of cells transfected with each plasmid were observed to possess leading processes directed toward the pial surface. These findings suggested that the radial migration of RYK- and dTK-expressing cells had been suppressed, but the cells expressing dLRM had migrated normally.

To confirm these observations, we analyzed the extent of radial cell migration quantitatively by dividing the cortex into five equal areas from the ventricular surface to the pial surface, and calculated the percentage of transfected cells in each area at 72 h after electroporation (Fig. 5). The results showed that the majority of the RYK-EGFP- and dTK-EGFP-expressing cells were located in the area closest to the ventricular surface, and smaller percentages of dLRM-EGFP- and EGFP-expressing cells were observed in the same area. By contrast, no RYK-EGFP- and dTK-EGFP-expressing cells were detected in the area closest to the pial surface,

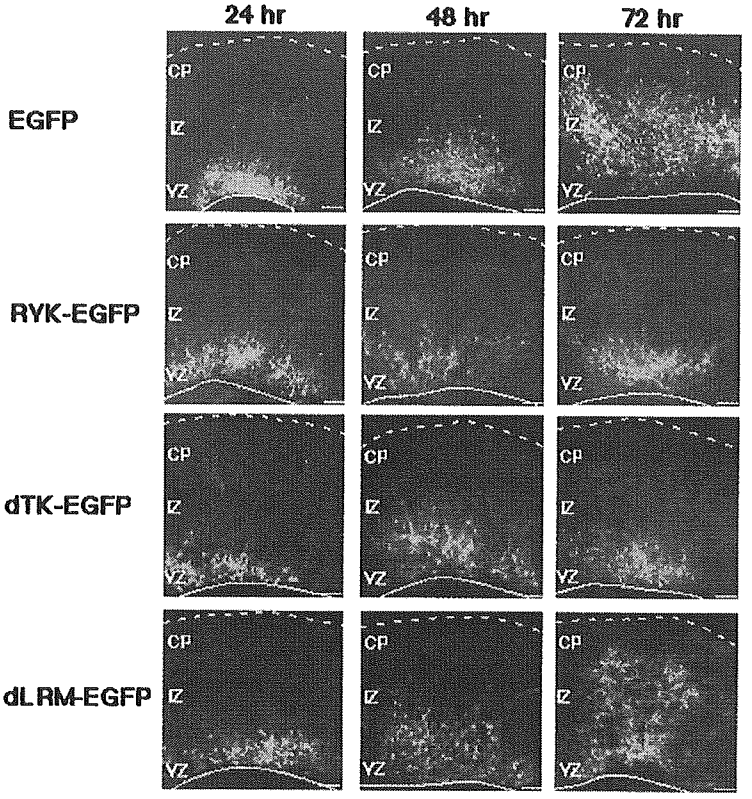

Fig. 4. Cell migration in neocortical slice culture. Expression plasmids for RYK-EGFP, dTK-EGFP, dLRM-EGFP, and control EGFP were electroporated into cells in the ventricular zone of E15, and cortical slice cultures were prepared. They were fixed and immunostained for GFP after 24, 48, and 72 h. The solid line represents the ventricular surface, and the broken line represents the pial surface. The radial migration of RYK- and dTK-expressing cells had been suppressed, but dLRM-expressing cells had migrated the same as EGFP-expressing cells. CP, cortical plate; IZ, intermediate zone; and VZ, ventricular zone. Scale bars, 100 μm.

but some of the dLRM-EGFP- and EGFP-expressing cells were detected in the same area. No RYK-EGFP-expressing cells and only a few dTK-EGFP-expressing cells were detected in the area second closest to the pial surface, whereas a large number of LRM-EGFP- and EGFP-expressing cells were observed in the same area. In the area third closest to the pial surface, which corresponds to the intermediate zone, the percentage of RYK-EGFP-expressing cells was lower than that of dTK-EGFP-expressing cells, and many more LRM-EGFP- and EGFP-expressing cells were observed in the same area. The results of the analyses confirmed suppression of the radial migration of RYK- and dTK-expressing cells, but cells expressing dLRM had migrated normally.

Discussion

During the development of the mammalian cerebral cortex, neural progenitor cells proliferate in the ventricular zone, post-mitotic neurons then migrate radially toward the pial surface. Several molecules have turned out to play key roles in each step of neuronal migration. For example, Lis1 and doublecortin regulate cytoskeletal formation, and the reelin pathway controls the stop signal for migrating cells [34–37]. Since ephrinB1 has been implicated in the regulation of cortical cell migration [28], molecules involved in the Eph signaling pathway may also play roles in this event. The interaction between RYK and EphB2/B3 [16,20], and the high expression of RYK in the ventricular zone [8,9] implied an important function of RYK in cortical development, and the finding in this study that hardly any RYK-overexpressing cells migrated out of the ventricular zone strongly suggests that RYK regulates the early step of cortical cell migration.

In this study, we showed that cells expressing dLRM, which is devoid of the LRMs of RYK, migrated normally in slice cultures, suggesting that LRMs are indispensable to the role of RYK in cell migration. The Western blot analyses suggested possible interaction between RYK and EphB2/B3 or ephrinB1/B2 in vivo, and LRMs were shown to be necessary for the binding of RYK to EphB3 in vitro. These findings suggested that RYK might regulate cortical cell migration through the Eph signaling pathway. Although the details of the molecular mechanism of the RYK/Eph signaling pathway in the regulation of cortical cell migration are currently unclear, it is possible that RYK and Eph

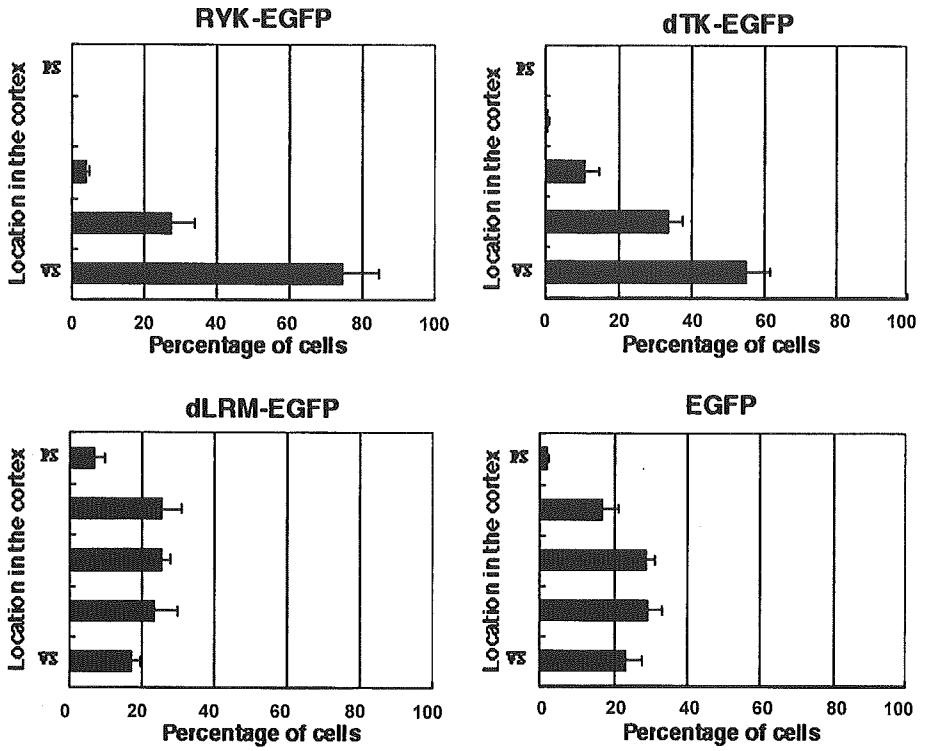

Fig. 5. Quantitative analyses of cell migration in slice cultures. Slice cultures were analyzed after incubation for 72 h. The cortex was subdivided evenly into five equal areas from the ventricular surface (VS) to the pial surface (PS), GFP-positive cells (cell bodies) in each area were counted, and the percentage of GFP-positive cells in each area was calculated. The results of the analyses confirmed suppression of the radial migration of RYK-expressing cells. Values are means ± SD. Five slices were used for each plasmid.

receptors suppress the cell migration cooperatively. Another explanation is that RYK may regulate cell migration by modulating the Eph signaling pathway, for example, RYK modulates the ligand affinity or the phosphorylation states of Eph receptors. RYK, EphB3, and ephrinB1/B2 are expressed in the ventricular zone of the embryonic cerebrum [17,28,38,39], and ephrins and Eph receptors are known to repel each other in many stages of neural development [17,21,22,40], implicating that RYK could modulate the repulsive effect between ephrins and Eph receptors that results in the regulation of cell migration.

Although no tyrosine kinase activity of RYK has ever been detected, a previous study has shown that mouse RYK binds to and can be phosphorylated by Eph receptors [16] whereas human RYK binds to, but is not phosphorylated by, Eph receptors [20], suggesting that the tyrosine-phosphorylation state of RYK differs with the species or cell type. We have therefore been interested in determining the significance of RYK phosphorylation during cortical cell migration, and we have investigated it by analyzing the RYK deletion mutant dTK, which lacks the tyrosine-kinase-related domain that contains six tyrosine residues. Surprisingly, dTK binds as tightly as full-length RYK to the Eph receptor in vitro. In addition, the migration of dTK-expressing cells was suppressed in slice cultures. These results indicate that the function of RYK during cell migration may be independent of phosphorylation. However, dTK still contains three tyrosine residues, and one of them may be the key phosphorylation site for the RYK activity during cell migration. Our preliminary study has shown the phosphorylation of RYK upon the co-transfection with EphB3 in vitro (data not shown). Further phosphorylation analysis of RYK (its deletion mutants as well) and Eph receptor would be required to examine the significance of phosphorylation of these molecules during cortical cell migration.

The results of the present study suggest that RYK and B-type Eph receptors form co-receptors and that ephrinBs could be the ligands during cortical cell migration. Meanwhile, the recent report showed that mammalian RYK functions as a receptor for Wnt in axon guidance [11], and during cortical cell migration, RYK could also participate in the Wnt signaling pathway. This pathway may be independent of the Eph cascade or signaling cross talk between Eph pathway and Wnt pathway may occur. Since dLRM also lacks a large part of the Wnt-inhibitory-factor-related domain (deleted 105 out of 129 amino acids) [7], the effect of dLRM-overexpression on the Wnt signaling pathway should be investigated in the future studies.

We are also interested in the intracellular molecules downstream of this signaling pathway. Three of the

molecules involved in the cortical cell migration, filamin A-interacting protein (FLIP), Rac1, and c-Jun N-terminal kinase (JNK), have been shown to regulate the early step of cell migration [41,42], and thus are candidates for downstream molecules in the RYK-mediated pathway. Further biochemical and in vivo analyses of the RYK-mediated signaling pathway should lead to elucidation of the molecular mechanism of cortical cell migration.

Acknowledgments

We thank Dr. Seisuke Hattori for providing us with plasmid pEphB3HA and Dr. Ryoichiro Kageyama for providing us with the retrovirus vector pCLIG. This study was supported by the Ministry of Health, Labour and Welfare of Japan.

References

[1] C.M. Hovens, S.A. Stacker, A.-C. Andres, A.G. Farpur, A. Ziemiecki, A.F. Wilks, RYK, a receptor tyrosine kinase-related molecule with unusual kinase domain motifs, Proc. Natl. Acad. Sci. USA 89 (1992) 11818–11822.

[2] S.A. Stacker, C.M. Hovens, A. Vitali, M.A. Pritchard, E. Baker, G.R. Sutherland, A.F. Wilks, Molecular cloning and chromosomal localization of the human homologue of a receptor related to tyrosine kinase (RYK), Oncogene 8 (1993) 1347–1356.

[3] R. Battye, A. Stevens, R.L. Perry, J.R. Jacobs, Repellent signaling by Slit requires the leucine-rich repeats, J. Neurosci. 21 (2001) 4290–4298.

[4] B. Kobe, A.V. Kajava, The leucine-rich repeat as a protein recognition motif, Curr. Opin. Struct. Biol. 11 (2001) 725–732.

[5] J.K. Bell, G.E. Mullen, C.A. Leifer, A. Mazzoni, D.R. Davies, D.M. Segal, Leucine-rich repeats and pathogen recognition in Toll-like receptors, Trends Immunol. 24 (2003) 528–533.

[6] J.C. Hsieh, L. Kodjabachian, M.L. Rebbert, A. Rattner, P.M. Smallwood, C.H. Samos, R. Nusse, I.B. Dawid, J. Nathans, A new secreted protein that binds to Wnt proteins and inhibits their activities, Nature 398 (1999) 431–436.

[7] L. Patthy, The WIF module, Trends Biochem. Sci. 25 (2000) 12–13.

[8] K. Kamitori, M. Machide, N. Osumi, S. Kohsaka, Expression of receptor tyrosine kinase RYK in developing rat central nervous system, Dev. Brain Res. 114 (1999) 149–160.

[9] K. Kamitori, M. Machide, K. Tomita, M. Nakafuku, S. Kohsaka, Cell-type-specific expression of protein tyrosine kinase-related receptor RYK in the central nervous system of rat, Mol. Brain Res. 104 (2002) 255–566.

[10] C.A. Callahan, M.G. Muralidhar, S.E. Lundgren, A.L. Scully, J.B. Thomas, Control of neuronal pathway selection by a *Drosophila* receptor protein-tyrosine kinase family member, Nature 376 (1995) 171–174.

[11] C. Moreau-Fauvarque, E. Taillebourg, E. Boissouneau, J. Mesnard, J.-M. Dura, The receptor tyrosine kinase gene *linotte* is required for neuronal pathway selection in *Drosophila* mushroom bodies, Mech. Dev. 78 (1998) 47–61.

[12] J.L. Bonkowsky, S. Yoshikawa, D.D. O'Keefe, A.L. Scully, J.B. Thomas, Axon routing across the midline controlled by the *Drosophila* Derailed receptor, Nature 402 (1999) 540–544.

[13] S. Yoshikawa, R.D. McKinnon, M. Kokel, J.B. Thomas, Wnt-mediated axon guidance via the *Drosophila* Derailed receptor, Nature 422 (2003) 583–588.

[14] T. Inoue, H.S. Oz, D. Wiland, S. Gharib, R. Deshpande, R.J. Hill, W.S. Katz, P.W. Sternberg, *C. elegans* LIN-18 is a Ryk ortholog and functions in parallel to LIN-17/Frizzled in Wnt signaling, Cell 118 (2004) 795–806.

[15] W. Lu, V. Yamamoto, B. Ortega, D. Baltimore, Mammalian Ryk is a Wnt coreceptor required for stimulation of neurite outgrowth, Cell 119 (2004) 97–108.

[16] M.M. Halford, J. Armes, M. Buchert, V. Meskenaite, D. Grail, M.L. Hibbs, A.F. Wilks, P.G. Farlie, D.F. Newgreen, C.M. Hovens, S.A. Stacker, Ryk-deficient mice exhibit craniofacial defects associated with perturbed eph receptor crosstalk, Nat. Genet. 25 (2000) 414–418.

[17] D. Orioli, M. Henkemeyer, G. Lemke, R. Klein, T. Pawson, Sek4 and Nuk receptors cooperate in guidance of commissural axons and in palate formation, EMBO J. 15 (1996) 6035–6049.

[18] A. Davy, J. Aubin, P. Soriano, Ephrin-B1 forward and reverse signaling are required during mouse development, Genes Dev. 18 (2004) 572–583.

[19] S.R.F. Twigg, R. Kan, C. Babbs, E.G. Bochukova, S.P. Robertson, S.A. Wall, G.M. Morriss-Kay, A.O.M. Wilkie, Mutations of ephrin-B1 (EFNB1), a marker of tissue boundary formation, cause craniofrontonasal syndrome, Proc. Natl. Acad. Sci. USA 101 (2004) 8652–8657.

[20] E. Trivier, T. Ganesan, RYK, catalytically inactive receptor tyrosine kinase, associates with EphB2 and EphB3 but dose not interact with AF-6, J. Biol. Chem. 277 (2002) 23037–23043.

[21] H.U. Wang, D.J. Anderson, Eph family transmembrane ligand can mediate repulsive guidance of trunk neural crest migration and motor axon outgrowth, Neuron 18 (1997) 383–396.

[22] J.G. Flanagan, P. Vanderhaegen, The ephrins and Eph receptors in neural development, Annu. Rev. Neurosci. 21 (1998) 309–345.

[23] J.C. Conover, F. Doetsch, J.-M. Garcia-Verdugo, N.W. Gale, G.D. Yancopoulos, A. Alvarez-Buylla, Disruption of Eph/ephrin signaling affects migration and proliferation in the adult subventricular zone, Nat. Neurosci. 3 (2000) 1091–1097.

[24] M.B. Delva, M.A. Takasu, M.Z. Lin, S.M. Shamah, L. Hu, N.W. Gale, M.E. Greenberg, EphB receptors interact with NMDA receptors and regulate excitatory synapse formation, Cell 103 (2000) 945–956.

[25] I.M. Ethell, F. Irie, M.S. Kalo, J.R. Couchman, E.B. Pasquale, Y. Yamaguchi, EphB/syndecan-2 signaling in dendritic spine morphogenesis, Neuron 3 (2001) 1001–1013.

[26] D.G. Wilkinson, Multiple roles of EPH receptors and ephrins in neural development, Nat. Rev. Neurosci. 2 (2001) 155–164.

[27] X. Zhou, J. Suh, D.P. Cerretti, R. Zhou, E. DiCicco-Bloom, Ephrins stimulate neurite outgrowth during early cortical neurogenesis, J. Neurosci. Res. 66 (2001) 1054–1063.

[28] I. Stuckmann, A. Weigmann, A. Shevchenko, M. Mann, W.B. Huttner, Ephrin B1 is expressed on neuroepithelial cells in correlation with neocortical neurogenesis, J. Neurosci. 21 (2001) 2726–2737.

[29] M. Hojo, T. Ohtsuka, N. Hashimoto, G. Gradwohl, F. Guillemot, R. Kageyama, Glial cell fate specification modulated by the bHLH gene *Hes5* in mouse retina, Development 127 (2000) 2515–2522.

[30] H. Tabata, K. Nakajima, Efficient *in utero* transfer system to the developing mouse brain using electroporation: visualization of neural migration in the developing cortex, Neuroscience 103 (2001) 865–872.

[31] T. Hirasawa, H. Wada, S. Kohsaka, S. Uchino, Inhibition of NMDA receptors induces delayed neuronal maturation and sustained proliferation of progenitor cells during neocortical development, J. Neurosci. Res. 74 (2003) 676–687.

[32] A.D. Bergemann, L. Zhang, M.K. Chiang, R. Brambilla, R. Klein, J.G. Flanagan, Ephrin-B3, a ligand for the receptor EphB3, expressed at the midline of the developing neural tube, Oncogene 16 (1998) 471–480.
[33] B. Nadarajah, J.E. Brunstrom, J. Grutzendler, R.O. Wong, A.L. Pearlman, Two modes of radial migration in early development of the cerebral cortex, Nat. Neurosci. 4 (2001) 143–150.
[34] M.E. Hatten, New direction in neuronal migration, Science 297 (2002) 1660–1663.
[35] Y. Feng, C.A. Walsh, Protein–protein interaction, cytoskeletal regulation and neuronal migration, Nat. Rev. Neurosci. 2 (2001) 408–416.
[36] A. Gupta, L.H. Tsai, A. Wynshaw-Boris, Life is a journey: a genetic look at neocortical development, Nat. Rev. Genet. 3 (2002) 342–355.
[37] E.C. Olson, C.A. Walsh, Smooth, rough and upside-down neocortical development, Curr. Opin. Genet. Dev. 12 (2002) 320–327.
[38] T. Ciossek, M.M. Lerch, A. Ullrich, Cloning, characterization, and differential expression of MDK2 and MDK5, two novel receptor tyrosine kinases of eck/eph family, Oncogene 11 (1995) 2085–2095.
[39] D.J. Liebl, C.J. Morris, M. Henkemeyer, L.F. Parada, mRNA expression of ephrins and Eph receptor tyrosine kinases in the neonatal and adult mouse central nervous system, J. Neurosci. Res. 7 (2003) 17–22.
[40] L.Q. Bundesen, T.A. Scheel, B.S. Bregman, L.F. Kromer, Ephrin-B2 and EphB2 regulation of astrocyte-meningeal fibroblast interaction in response to spinal cord lesions on adult rats, J. Neurosci. 23 (2003) 7789–7800.
[41] T. Nagano, T. Yoneda, Y. Hatanaka, C. Kubota, F. Murakami, M. Sato, Filamin A-interacting protein (FLIP) regulates cortical cell migration out of the ventricular zone, Nat. Cell. Biol. 4 (2002) 495–501.
[42] T. Kawauchi, K. Chihama, Y. Nabeshima, M. Hoshino, The in vivo roles of STEF/Tiam1, Rac1, and JNK in cortical neuronal migration, EMBO J. 22 (2003) 4190–4201.

Journal of Neuroscience Research 81:357–362 (2005)

Visualization of Microglia in Living Tissues Using Iba1-EGFP Transgenic Mice

T. Hirasawa, K. Ohsawa, Y. Imai, Y. Ondo, C. Akazawa, S. Uchino, and S. Kohsaka*

Department of Neurochemistry, National Institute of Neuroscience, Kodaira, Tokyo, Japan

Microglia are thought to play important roles not only in repairing injured tissue but in regulating neuronal activity, and visualizing the cells is very useful as a means of further investigating the function of microglia in vivo. We previously cloned the ionized calcium-binding adaptor molecule 1 (*Iba1*) gene, which is expressed selectively in microglia/microphages. To generate new transgenic mice to visualize microglia with enhanced green fluorescent protein (EGFP), we here constructed a plasmid carrying EGFP cDNA under control of the *Iba1* promoter. This construct was injected into C57B/6 mouse zygotes, and the Iba1-EGFP transgenic line was developed. Fluorescent in-situ hybridization analysis revealed that the *Iba1-EGFP* transgene was located on chromosome 11D. No obvious defects were observed during development or in adulthood, and the EGFP fluorescence remained invariant over the course of at least four generations. Judging from the immunoreactivity with anti-Iba1 antibody, all EGFP-positive cells in the adult brain were ramified microglia. In the developing transgenic embryos, EGFP signals were detected as early as embryonic Day 10.5. The most prominent EGFP signals were found in forebrain, spinal cord, eye, foreleg, yolk sac, liver, and vessel walls. At postnatal Day 6, clear EGFP signals were observed in the supraventricular corpus callosum, known as "fountain of microglia," where ameboid microglia migrate into the brain parenchyma and mature into ramified microglia. Iba1-EGFP transgenic mice thus permit observation of living microglia under a fluorescence microscope and provide a useful tool for studying the function of microglia in vivo. © 2005 Wiley-Liss, Inc.

Key words: Iba1; EGFP; microglia; visualization

Microglia are the resident macrophages in the brain and are thought to modulate the pathologic and regenerative states of the brain by producing a variety of molecules including neurotrophic and neurotoxic factors (Kreutzberg, 1996; Nakajima and Kohsaka, 2001, 2004). Resident microglia have been observed in the developing brain even in 10-day-old embryo (E10) rat brain (Abney et al., 1981; Fedoroff and Hao, 1991). Morphologically, these cells do not have processes, and referred to as ameboid microglia. The cell density of this population is sustained at low levels before neurogenesis. The microglia increase in number in association with neurogenesis and subsequent gliogenesis, and develop morphologically. Cumulative evidence has shown that microglia at this stage play a role in the regulation of cell differentiation, cell number, synapse formation, and tissue clearance (Nagata et al., 1993; Hamilton and Rome, 1994; Cammer and Zhang, 1996; Miller and Kaplan, 2001; Farinas et al., 2002; Markus et al., 2002). From this stage until adulthood, they morphologically change into ramified microglia, which have many fine perpendicular processes extending from a few long prolongations, and uniformly disperse throughout the brain. This type of microglia generally has been considered functionally inactive or in a resting state, and they have been regarded as sensor cells whose function is to detect abnormalities or changes in the brain (Kreutzberg, 1996). When the brain is injured or affected by diseases, such as ischemia or neurodegenerative disease, the ramified microglia at the affected site morphologically transform into cells with retracted processes and enlarged cell bodies, and they increase in number (Kreutzberg, 1996). Microglia with this particular cell form are generally referred to as activated or reactive microglia (Streit et al., 1999). The conventional methods that use immunostaining techniques thus have shown that the morphology, cell number, and distribution of the resident microglia change during development and are altered by injury and disease. The process of these changes, however, has not been well understood.

Recent advances in techniques that use enhanced green fluorescent protein (EGFP) to visualize particular cells or protein molecules in situ make it possible to investigate cell morphology, the dynamics of target proteins, and their regulation in living tissues and cells. In

Contact grant sponsor: Ministry of Health, Labor and Welfare, Japan; Contract grant sponsor: Japan Health Sciences Foundation.

Y. Imai is currently at the Division of Molecular Cellular Physiology, Department of Molecular Cellular Biology, School of Medicine, Ehime University, Shigenobu, Onsen-gun, Ehime 791-0295, Japan.

*Correspondence to: Shinichi Kohsaka, Department of Neurochemistry, National Institute of Neuroscience, 4-1-1 Ogawahigashi, Kodaira, Tokyo 187-8502, Japan. E-mail: kohsaka@ncnp.go.jp

Received 2 September 2004; Accepted 15 September 2004

Published online 9 June 2005 in Wiley InterScience (www.interscience.wiley.com). DOI: 10.1002/jnr.20480

© 2005 Wiley-Liss, Inc.

combination with genome engineering, generation of the transgenic mice expressing EGFP in target cells is a very useful tool for studying cell properties in situ. For example, transgenic mice carrying EGFP under the control of the astrocyte-specific glial fibrillary acidic protein (GFAP) promoter have revealed the dynamic changes in astrocyte morphology during development (Zhuo et al., 1997; Nolte et al., 2001). In addition, the identification and characterization of neural stem cells not only in embryos but in adult brain has been achieved by using transgenic mice carrying EGFP under the control of the nestin second-intronic enhancer (Kawaguchi et al., 2001; Mignone et al., 2004). We therefore tried to produce transgenic mice in which microglia can be visualized in situ as a means of studying the properties of microglia during development, including changes in morphology, cell number, and distribution.

To achieve this end, we used the promoter of the ionized calcium-binding adaptor molecule 1 (*Iba1*) gene. Iba1, which is identical to allograft inflammatory factor-1 (AIF-1) (Utans et al., 1995) and balloon angioplasty responsive transcription-1 (BART-1) (Autieri et al., 1996), is a 17-kDa protein containing two EF-hand motifs, is expressed selectively in microglia/macrophages (Imai et al., 1996). We generated transgenic mice carrying EGFP under the control of the *Iba1* promoter and demonstrated that the microglia/macrophages of these transgenic mice specifically expressed EGFP. In the present study, we developed a valuable tool for visualize microglia/macrophages throughout the body and in living tissue.

MATERIALS AND METHODS

Transgene Construction

A genomic gene of mouse Iba1 was cloned from a129Sv/J mouse cosmid library (Stratagene; GenBank accession number AB036423). The transgene construct was prepared by subcloning the 1.9-kb *Eco*RI-*Hin*dIII fragment from the 5′-flanking region of the *Iba1* gene (position 2178–4066), including exon 1, intron 1, and a portion of exon 2, fused with a cDNA of EGFP and a polyadenylation (poly-A) sequence of simian virus 40 from pIRES-EGFP (Clontech, Palo Alto, CA) into the pBluescript II SK(−) vector, generating Iba1-EGFP plasmid. This transgene construct was designed to add 17 additional amino acids to the N-terminal of EGFP, whose expression was controlled by the *Iba1* promoter.

Cell Culture and Transfection

THP-1 cells (a human acute monocytic leukemic cell line, Tsuchiya et al., 1980) and COS-7 (a monkey kidney epithelium cell line) cells were grown in RPMI1640 (Gibco BRL, Grand Island, NY) and Dulbecco's modified Eagle medium (DMEM; Gibco BRL), respectively, containing 10% heat-inactive fetal bovine serum (FBS; Irvine, Santa Ana, CA), at 37°C under a humidified 5% CO_2 atmosphere. For the transient expression studies, THP-1 cells and COS-7 cells were transfected with expression plasmid by electroporation with GenePulser (Bio-Rad) and by using Lipofectamine Plus (Gibco BRL), respectively, as indicated in the manufacturer's protocol.

Generation and Genotyping of Iba1-EGFP Transgenic Mice

Transgenic mice were generated by pronuclear microinjection of fertilized C57BL/6 strain oocytes. To identify founder mice, the genotypes of all offspring were analyzed by polymerase chain reaction (PCR) as follows. Genomic DNA was prepared from tail biopsies. The thermocycle profile for PCR amplification was: 1 min at 94°C, 1 min at 55°C, and 2 min at 72°C for 40 cycles. The primers for PCR analysis were: sense primer for Iba1 gene and transgene, 5′-TACCGC-ATCCTTGGTTTGAG-3′; anti-sense primer for Iba1 gene, 5′-CTTGTTGATCCCCTCCAGCC-3′; and anti-sense primer for transgene, 5′-CTTGTACAGCTCGTCCATGC-3′. The PCR products, a 0.8-kb fragment of the genomic Iba1 gene and a 1.5-kb fragment of the transgene, were separated on a 0.7% agarose gel and stained with ethidium bromide.

Fluorescent In Situ Hybridization Analysis

Fluorescent in situ hybridization (FISH) analysis of the chromosomes from the mice was carried out as described previously (Matsuda et al., 1992). Briefly, the cDNA of EGFP was labeled with biotin-16-dUTP with a nick translation kit (Roche, Germany). After overnight hybridization, the signals were detected with fluorescein isothiocyanate (FITC)-conjugated avidin (Roche). Counterstaining was carried out with propidium iodide (PI) and Hoechst 33258.

Preparation of Living Slices and Microtome Sections

Living slices were prepared as follows. The dissected brain was placed on 3% agarose, then cut into 200- to 400-μm sections in ice-cold Tyrode's solution (in mM: 136.8 NaCl, 2.5 KCl, 1.7 $CaCl_2$, 1.0 $MgCl_2$, 0.38 Na_2PO_4, 11.9 $NaHCO_3$, and 5.5 glucose) with a microtome VT-1000S (Leica, Germany), and examined with a fluorescence stereoscopic microscope MZFL III (Leica).

Microtome sections were prepared as follows. The dissected brains were fixed with 4% paraformaldehyde (PFA) at 4°C for 16 hr. After washing in phosphate-buffered saline (PBS) for 20 min, the brains were cut into 50-μm sections in PBS with a microtome.

The experimental protocols were approved by The Animal Care and Use Committee of National Institute of Neuroscience.

Immunohistochemistry

The dissected brains were fixed with 4% PFA at 4°C for 16 hr. After washing in PBS for 20 min, the brains were equilibrated in 20% sucrose in PBS, embedded in optimal cutting temperature (OTC) compound, and frozen in dry ice. The frozen brains were cut into 14-μm sections with a cryostat CM-3000 (Leica), and the sections were mounted onto 3-aminopropyltriethoxysilane (APS)-coated glass slides (Matsunami, Osaka, Japan). The sections were permeabilized and blocked with 3% goat serum-0.1% Triton X-100 in PBS for 20 min, and then stained with rabbit polyclonal anti-Iba1 (2 μg/ml). After three washes with PBS, the sections were incubated for 1 hr at room temperature with Alexa Fluor594-goat anti-rabbit IgG (H+L, 1:1,000; Molecular Probes, Eugene, OR) in PBS

containing 3% bovine serum albumin. The sections were then mounted on a glass slide with PermaFluor (Thermo Shandon, Pittsburgh, PA) and examined with an AX70 fluorescence microscope (Olympus, Tokyo, Japan).

RESULTS

Generation of Iba1-EGFP Transgenic Mice

To obtain the promoter of the mouse *Iba1* gene, we isolated Iba1 genomic DNA from a 129Sv/J mouse cosmid library. Sequencing analysis revealed that Iba1 gene consists of six exons, and that five interferon-γ (IFNγ)-responsive elements (IREs) are present in the upstream of the second exon (Fig. 1A). A previous study showed that the restricted expression of *Iba1* in microglia/macrophage is enhanced by IFNγ, suggesting that the expression of Iba1 is controlled by IRE (Imai and Kohsaka, 2002; Sibinga et al., 2002). To determine whether the *Eco*RI-*Hind*III 1.9-kb *Iba1* genomic fragment containing IRE shown in Figure 1A functions as a promoter, we constructed a plasmid in which a cDNA of EGFP and a poly-A sequence were placed downstream of the 1.9-kb *Iba1* genomic fragment. Because Iba1 is expressed in a human acute monocytic leukemia cell line, THP-1 cells, but not in COS-7 cells, the plasmid was introduced into THP-1 cells and COS-7 cells (Imai et al., 1996). As expected, the EGFP fluorescence was detected only in the THP-1 cells (Fig. 1B), indicating that the 1.9-kb Iba1 genomic fragment was sufficient to function as a promoter in THP-1 cells as well as an endogenous Iba1 promoter. This observation prompted us to use this construct as a novel marker of microglia in brain to visualize microglia/macrophages. After injection of the construct into C57BL/6 mouse zygotes, seven transgenic lines were obtained. One line determined by genotyping analysis and EGFP fluorescence was then chosen for subsequent analysis. No obvious defects were detected during development or in adulthood, and the EGFP fluorescence remained invariant over the course of at least four generations. We then carried out FISH analysis to identify the site where the *Iba1-EGFP* transgene had been integrated into the chromosomes, and as shown in Figure 1C, the twin-spot FITC signals of the *Iba1-EGFP* transgene were detected on chromosome 11D.

EGFP-Positive Cells in the Adult Brain of Iba1-EGFP Transgenic Mice Were Identified As Microglia

We initially examined the living brain slices prepared from the adult Iba1-EGFP transgenic mice for EGFP fluorescence. Under a simple light transmission mode at low magnification, the slices appeared bright but when the same field was illuminated with a laser beam, they emitted strong diffuse fluorescence (Fig. 2A). The slices prepared from the nontransgenic mice, however, showed no signals (data not shown), indicating that the observed fluorescence was the EGFP signal, not autofluorescence. At higher magnification, fluorescence was observed throughout the brain slices and matched

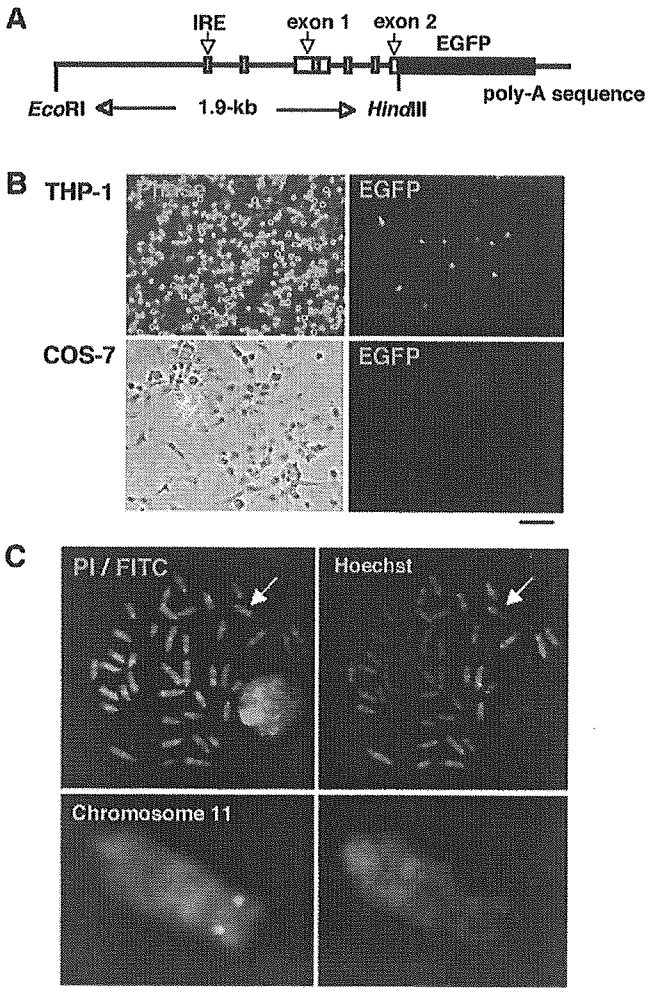

Fig. 1. Iba1-enhanced green fluorescent protein (EGFP) transgenic mice. **A:** Schematic of the Iba1-EGFP transgene construct. The 1.9-kb *Eco*R1-*Hind*III fragment from the 5′-flanking region of Iba1 gene including exon 1, intron 1, and a portion of exon 2 was fused with EGFP cDNA (black box) and a polyadenylation sequence. The five red boxes represent the interferon-γ responsive elements (IREs). **B:** Transfection of the Iba1-EGFP transgene construct into THP-1 cells and COS-7 cells. A phase-contrast image (left panel) and EGFP fluorescence image (right panel) are shown. Scale bar = 50 μm. **C:** Fluorescent in situ hybridization (FISH) analysis. The chromosomal location of Iba1-EGFP transgene is indicated by the arrow. The left panels show the FITC signals, indicating that the Iba1-EGFP transgene merged with R-banded chromosomes stained with propidium iodide (PI). The right panels show G-banded chromosomes stained with Hoechst 33258 (Hoechst). The lower panels show chromosome 11 at higher magnification.

the distribution of microglia detected by immunostaining (Fig. 2B). When examined with a 40× objective, the cells emitting EGFP fluorescence were concluded to be ramified microglia based on their morphology (Fig. 2C).

We next investigated whether EGFP expression in the brain is controlled precisely by the *Iba1* promoter by carrying out an immunohistochemical analysis with anti-Iba1 antibody. As shown in Figure 2D, the EGFP-positive cells were observed uniformly throughout the brain,

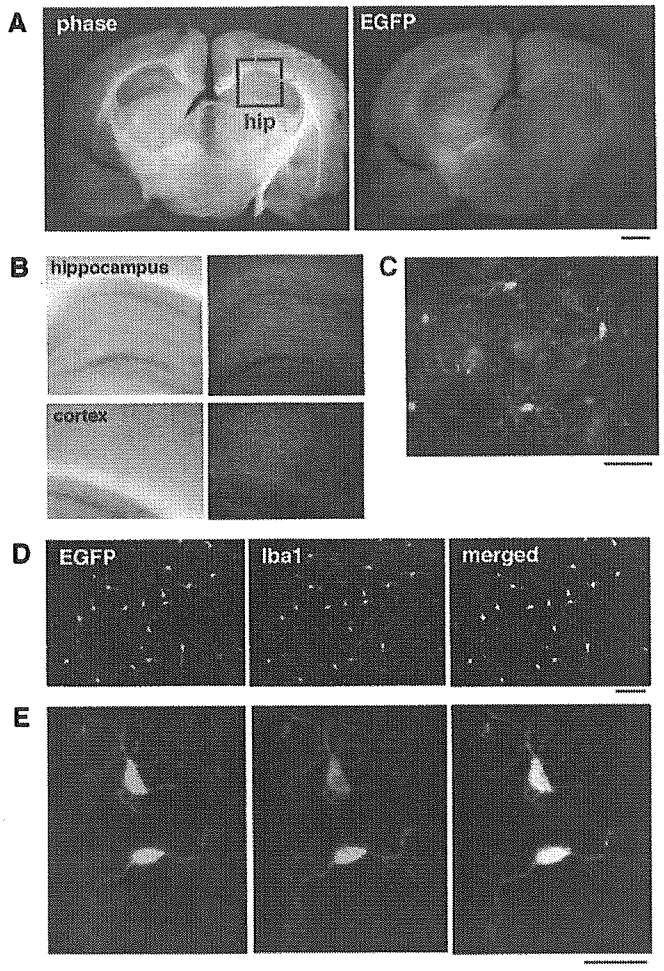

Fig. 2. Enhanced green fluorescent protein (EGFP) fluorescence in the brain of adult Iba1-EGFP transgenic mice. **A:** Microtome section. A phase-contrast image (left panel) and EGFP fluorescence image (right panel) are shown. Scale bar = 1 mm. hip, hippocampus; cx, cortex. **B:** Hippocampus and cortex enclosed by boxes in A are shown at higher magnification. A phase-contrast image (left panel) and EGFP fluorescence image (right panel) are shown. **C:** EGFP-positive cells in the cortex are shown at higher magnification. Scale bar = 50 μm. **D, E:** Microphotographs of immunohistochemically stained brain section with anti-Iba1 antibody. EGFP-positive cells completely matched with Iba1-expressing ramified microglia. Scale bar = 100 μm (D); 25 μm (E).

and all were immunoreactive for anti-Iba1 antibody. At higher magnification, the EGFP-expressing cells were found to be typical ramified microglia (Fig. 2E). EGFP expression in the Iba1-EGFP transgenic mice thus paralleled Iba1 expression in the adult brain. Because Iba1 is expressed selectively in microglia, we concluded that the *Iba1-EGFP* transgene was expressed in microglia.

EGFP Expression in the Transgenic Mice During Development

EGFP signals were detected in the developing Iba1-EGFP transgenic embryos as early as E10.5 (Fig. 3A). At

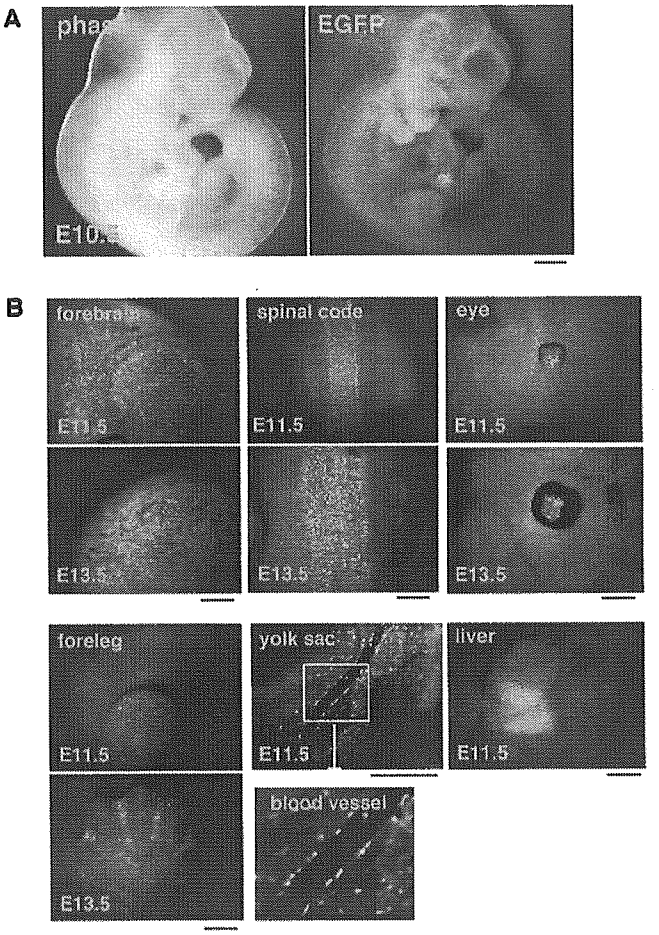

Fig. 3. Enhanced green fluorescent protein (EGFP) fluorescence in Iba1-EGFP transgenic mouse embryos. **A:** Whole embryonic Day 10.5 (E10.5) embryo. A phase-contrast image (left panel) and EGFP fluorescence image (right panel) are shown. Scale bar = 500 μm. **B:** EGFP fluorescence images in specific regions at E11.5 and E13.5 embryos. Forebrain, spinal cord, eye, foreleg, yolk sac, and liver are shown. The blood vessel enclosed in yolk sac is shown at higher magnification. Scale bar = 500 μm.

E11.5, prominent EGFP signals were observed in the forebrain, spinal cord, eye, foreleg, yolk sac, liver, and vessel walls. As embryonic development proceeded, the intensity of EGFP fluorescence gradually increased from day to day (Fig. 3B). At this stage, the EGFP-positive cells in the brain were distributed mainly on the pial surface.

In the early postnatal stage, microglial cells invade the brain from specific areas, such as the supraventricular corpus callosum. These invading ameboid microglia migrate into the brain parenchyma where they ultimately mature to ramified microglia (Imamoto and Leblond, 1978; Ling, 1979). We then examined the EGFP signals in the Iba1-EGFP transgenic mice at postnatal Day 6 (P6). As shown in Figure 4A, clear EGFP signals were observed in the supraventricular corpus callosum, and morphologically the EGFP-positive cells were the ameboid type (Fig. 4B). As development proceeded, the

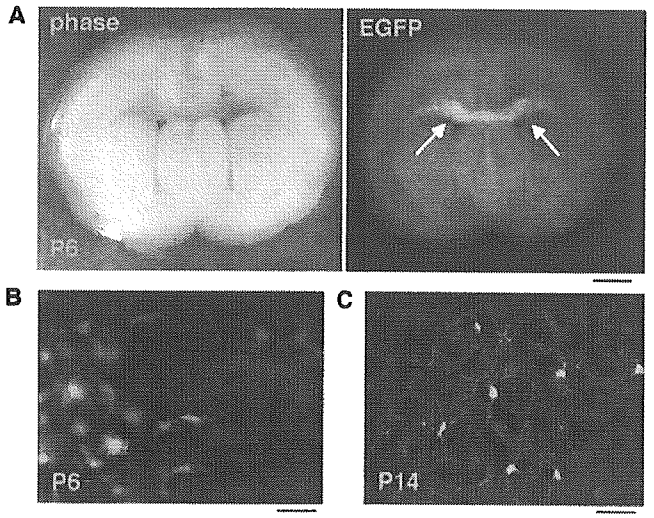

Fig. 4. Enhanced green fluorescent protein (EGFP) fluorescence in Iba1-EGFP transgenic mice. **A:** Microtome section at mouse stage postnatal Day 6 (P6). A phase-contrast image (left panel) and EGFP fluorescence image (right panel) are shown. The supraventricular corpus callosum is indicated by arrows. Scale bar = 1 mm. **B, C:** EGFP-positive cells in the supraventricular corpus callosum in a P6 (B) and in the cortex in a P14 (C) mouse are shown at higher magnification. Scale bar = 50 μm.

EGFP-positive cells in this area decreased in number, and eventually failed to be detected in the P14 transgenic mice (data not shown), and the EGFP-positive cells in the cortical parenchyma became mature ramified microglia (Fig. 4C).

DISCUSSION

Immunostaining with antibody is a conventional technique for studying the properties of microglia. Because its application is restricted to fixed tissues, i.e., dead cells, however, it is difficult to identify accurately dynamic changes in developing microglia. To overcome this problem, we generated transgenic mice with expression of EGFP under the control of the *Iba1* promoter. Because this promoter selectively functions in microglia/macrophages (Imai et al., 1996), microglia/macrophages in living tissues can be labeled with EGFP fluorescence. To verify that the EGFP-expressing cells in the brain were indeed microglia, we immunostained the same sections for Iba1 and confirmed that all EGFP-expressing cells were also labeled with anti-Iba1 antibody. We therefore concluded that the Iba1-EGFP transgenic mice permit visualization of microglia in living brain tissue.

It is well known that ameboid microglia, which exhibit immature features, migrate through the brain parenchyma during differentiation and transform into mature ramified microglia when they reach their final location (Ling and Wong, 1993; Cuadros and Navascués, 1998; Dalmau et al., 2003). We used Iba1-EGFP transgenic mice to confirm that EGFP-positive cells in the brain in the embryonic stage were of the ameboid form, but were of the ramified form in adult brain. Despite great effort, however, the ontogenesis of microglia remains a matter of controversy and awaits elucidation. Previous reports have led to two hypotheses for the origin of microglia: a neuroectodermic origin and a mesodermal origin. In the latter hypothesis, hematopoietic cell-derived precursors, such as primitive macrophages and monocytes, have been proposed as the cells of origin of microglia. These cells are thought to enter the developing brain from the bloodstream, the ventricular spaces, or the meninges (Ling and Wong, 1993; Cuadros and Navascués, 1998, 2001; Dalmau et al., 2003). The Iba1-EGFP transgenic mice allow visualization of microglia after E10.5. The yolk sac and liver were among the organs that emitted prominent EGFP fluorescence, corroborating the results of a previous study showing that microglial progenitors originate from the yolk sac and are carried to the brain from hematopoietic organs, such as the liver, by the bloodstream (Alliot et al., 1999). In the embryonic stage, the EGFP-positive cells in the brain were detected mainly on the pial surface, and this finding is consistent with the proposal that the meninges is one of the entry routes for microglia into the brain parenchyma (Cuadros and Navascués, 1998). Although microglia mainly invade the brain parenchyma in the prenatal period, a smaller population invades postnatally, at P5–10. This late invasion is restricted to particular areas, such as the cingulum and the supraventricular corpus callosum, which is known to represent a "fountain of microglia" (Imamoto and Leblond, 1978; Ling, 1979). Using the Iba1-EGFP transgenic mice at P6 in this study enabled us to confirm that the strong EGFP signals originated in the ameboid microglia in the supraventricular corpus callosum. The living tissues of Iba1-EGFP transgenic mice can thus be used to analyze the ontogenesis of microglia. We also believe that they will be useful for visualizing dynamic changes in microglia during physiologic processes, such as cell proliferation and phagocytic behavior, in real time.

Iba1-EGFP transgenic mice exhibited different phenotypes of EGFP fluorescence depending on their parental origin. The mice carrying the paternally inherited transgene displayed a robust EGFP signal, whereas the mice carrying the maternally inherited transgene displayed little or no signal. FISH analysis revealed that the *Iba1-EGFP* transgene was located on chromosome 11D, where it has been suggested to be imprinted (Monk et al., 2003). Although the cause of the different phenotypes is unclear, the differential expression of the Iba1-EGFP transgene may be caused by intrinsic genomic imprinting of the *Iba1* gene. Further study will be needed to answer this question.

ACKNOWLEDGMENTS

We thank Dr. K. Goto (Central Institute for Experimental Animals) for help with the FISH analysis, and Dr. T. Kubota (University of Yamanashi) for valuable discussion and advice.

REFERENCES

Abney ER, Bartlett PP, Raff MC. 1981. Astrocytes, ependymal cells, and oligodendrocytes develop on schedule in dissociated cell cultures of embryonic rat brain. Dev Biol 83:301–310.

Alliot F, Godin I, Pessac B. 1999. Microglia derive from progenitors, originating from the yolk sac, and which proliferate in the brain. Brain Res Dev Brain Res 117:145–152.

Autieri MV, Prystowsky MB, Ohlstein EH. 1996. Isolation and characterization of BART-1: a novel balloon angioplasty responsive transcript in rat carotid arteries. DNA Cell Biol 15:297–304.

Cammer W, Zhang H. 1996. Carbonic anhydrase II in microglia in forebrains of neonatal rats. J Neuroimmunol 67:131–136.

Cuadros M, Navascués J. 1998. The origin and differentiation of microglial cells during development. Prog Neurobiol 56:173–189.

Cuadros M, Navascués J. 2001. Early origin and colonization of the developing central nervous system by microglial precursors. In: Castellano B, Nieto-Sampedro M, editors. Glial cell function. Amsterdam: Elsevier. p 51–59.

Dalmau I, Vela JM, González B, Finsen B, Castellano B. 2003. Dynamics of microglia in the developing rat brain. J Comp Neurol 458:144–157.

Farinas I, Cano-Jaimez M, Bellmunt E, Soriano M. 2002. Regulation of neurogenesis by neurotrophins in developing spinal sensory ganglia. Brain Res Bull 57:809–816.

Fedoroff S, Hao C. 1991. Origin of microglia and their regulation by astroglia. Adv Exp Med Biol 296:135–142.

Hamilton SP, Rome LH. 1994. Stimulation of in vitro myelin synthesis by microglia. Glia 11:326–335.

Imai Y, Ibata I, Ito D, Ohsawa K, Kohsaka S. 1996. A novel gene iba1 in the major histocompatibility complex class III region encoding an EF hand protein expressed in a monocytic lineage. Biophys Biochem Res Commun 224:855–862.

Imai Y, Kohsaka S. 2002. Intracellular signaling in M-CSF-induced microglial activation: role of Iba1. Glia 40:164–174.

Imamoto K, Leblond CP. 1978. Radioautographic investigation of gliogenesis in the corpus callosum of young rat. II. Origin of microglial cells. J Comp Neurol 180:139–164.

Kawaguchi A, Miyata T, Sawamoto K, Takashita N, Murayama A, Akamatsu W, Ogawa M, Okabe M, Tano Y, Goldman SA, Okano H. 2001. Nestin-EGFP transgenic mice: visualization of the self-renewal and multipotency of CNS stem cells. Mol Cell Neurosci 17:259–273.

Kreutzberg GW. 1996. Microglia: a sensor for pathological events in the CNS. Trends Neurosci 19:312–318.

Ling EA. 1979. Transformation of monocytes into ameboid microglia in the corpus callosum of postnatal rats, as shown by labeling monocytes by carbon particles. J Anat 128:847–858.

Ling EA, Wong WC. 1993. The origin and nature of ramified and ameboid microglia: a historical review and current concepts. Glia 7:9–18.

Markus A, Patel TD, Snider WD. 2002. Neurotrophic factors and axonal growth. Curr Opin Neurobiol 12:523–531.

Matsuda Y, Harada YN, Natsune-Sakai S, Lee K, Shiomi T, Chapman VM. 1992. Location of the mouse complement factor H gene (cfh) by FISH analysis and replication R-banding. Cytogenet Cell Genet 61: 282–285.

Mignone JL, Kukekov V, Chiang AS, Steindler D, Enikolopov G. 2004. Neural stem and progenitor cells in nestin-GFP transgenic mice. J Comp Neurol 469:311–324.

Miller FD, Kaplan DR. 2001. Neurotrophin signaling pathways regulating neuronal apoptosis. Cell Mol Life Sci 58:1045–1053.

Monk D, Smith R, Arnaud P, Preece MA, Stanier P, Beechey CV, Peters J, Kelsey G, Moore GE. 2003. Imprinted methylation profiles for proximal mouse chromosomes 11 and 7 as revealed by methylation-sensitive representational difference analysis. Mamm Genome 14: 805–816.

Nagata K, Takei N, Nakajima K, Saito H, Kohsaka S. 1993. Microglial conditioned medium promotes survival and development of cultured mesencephalic neurons from embryonic rat brain. J Neurosci Res 34: 357–363.

Nakajima K, Kohsaka S. 2001. Microglia: activation and their significance in the central nervous system. J Biochem 130:169–175.

Nakajima K, Kohsaka S. 2004. Microglia: neuroprotective and neurotrophic cells in the central nervous system. Curr Drug Targets Cardiovasc Haematol Disord 4:65–84.

Nolte C, Matyash M, Pivneva T, Schipke CG, Ohlemeyer C, Hanisch UK, Kirchhoff F, Kettenmann H. 2001. GFAP promoter-controlled EGFP-expressing transgenic mice: a tool to visualize astrocytes and astrogliosis in living brain tissue. Glia 33:72–86.

Sibinga NE, Feinberg MW, Yang H, Werner F, Jain MK. 2002. Macrophage-restricted and interferon γ-inducible expression of the allograft inflammatory factor-1 gene requires Pu.1. J Biol Chem 277:16202–16210.

Streit WJ, Walter SA, Pennell NA. 1999. Reactive microgliosis. Prog Neurobiol 57:563–581.

Tsuchiya S, Yamabe M, Yamaguchi Y, Kobayashi Y, Konno T, Tada K. 1980. Establishment and characterization of a human acute monocytic leukemia cell line (THP-1). Int J Cancer 26:171–176.

Utans U, Arceci RJ, Yamashita Y, Russell ME. 1995. Cloning and characterization of allograft inflammatory factor-1: a novel macrophage factor identified in rat cardiac allografts with chronic rejection. J Clin Invest 95:2954–2962.

Zhuo L, Sun B, Zhang CL, Fine A, Chiu SY, Messing A. 1997. Live astrocytes visualized by green fluorescent protein in transgenic mice. Dev Biol 187:36–42.

THE JOURNAL OF BIOLOGICAL CHEMISTRY VOL. 280, NO. 50, pp. 41619–41627, December 16, 2005
© 2005 by The American Society for Biochemistry and Molecular Biology, Inc. Printed in the U.S.A.

Ubiquitylation and Degradation of Serum-inducible Kinase by hVPS18, a RING-H2 Type Ubiquitin Ligase*

Received for publication, August 1, 2005, and in revised form, September 15, 2005 Published, JBC Papers in Press, October 3, 2005, DOI 10.1074/jbc.M508397200

Satomi Yogosawa[‡§], Shigetsugu Hatakeyama[¶], Keiichi I. Nakayama[‖], Hiroyuki Miyoshi[**], Shinichi Kohsaka[‡1], and Chihiro Akazawa[‡]

From the [‡]Department of Neurochemistry, National Institute of Neuroscience, National Center of Neurology and Psychiatry, Tokyo 187-8502, Japan, [§]Division of Molecular Life Science, School of Life Science, Tokyo University of Pharmacy and Life Science, Tokyo 192-0392, [¶]Department of Molecular Biochemistry, Hokkaido University Graduate School of Medicine, Sapporo 060-8638, [‖]Department of Molecular and Cellular Biology, Medical Institute of Bioregulation, Kyushu University, CREST, Japan Science and Technology Agency, Fukuoka 812-8582, [**]Subteam for Manipulation of Cell Fate, Bio Resource Center, RIKEN, Tsukuba 305-0074, Japan

Serum-inducible kinase (SNK) is a member of polo-like kinases that serve as regulators of multiple events during cell division. Rapid changes in the activity and abundance of SNK were reported after the serum stimulation and after the activation of synaptic transmission in the brain. Yet the detailed mechanisms that control the level of SNK protein have not been fully elucidated. In this report, we show that the RING-H2 domain of hVPS18 (human vacuolar protein sorting 18) has a genuine ubiquitin ligase (E3) activity. Using the yeast two-hybrid screening, we identify SNK as a candidate substrate of hVPS18. The half-life of SNK is increased in HeLa cells that down-regulated hVPS18 by lentivirus-mediated small hairpin RNA interference. Furthermore, the delayed entry into S phase is observed in HeLa cells overexpressing hVPS18. These results suggest that hVPS18 may play an important role in regulation of SNK activity through its ubiquitin ligase.

The polo-like kinases are a family of serine/threonine protein kinases that include mammalian polo-like kinase (Plk)1,[2] SNK (Plk2), fibroblast growth factor (Plk3), Sak (Plk4), *Caenorhabditis elegans* Plc1–3, *Xenopus laevis* Plx1, *Drosophila* polo, fission yeast Plo1, and budding yeast Cdc5 (1). Genetic and biochemical evidence in various organisms indicates that polo-like kinases play pivotal roles in regulating many cell-cycle dependent processes such as centrosome maturation and separation, mitotic entry, metaphase to anaphase transition, mitotic exit, and cytokinesis (2, 3). A number of studies (4, 5) suggest that the kinase activity is regulated by a variety of post-translational processes, including phosphorylation and ubiquitin conjugation.

The mammalian homologues of yeast Class C type of vacuolar protein sorting (VPS) proteins appear to control the fusion events of late endosomes and lysosomes that are the major pathway of the intracellular protein degradation (6, 7). There are four genes in human Class C *VPS*: *hVPS11*, *hVPS16*, *hVPS18*, and *hVPS33*. Studies of the domains of hVPS11 and hVPS18 have consistently revealed the existence of a RING-H2 motif, a member of RING fingers, located near the C-terminal. RING-H2 finger domains are present in a wide variety of proteins, and in the recent past it has been found that several RING-H2 finger proteins take part in the ubiquitin-proteasome pathway by playing as E3 ubiquitin ligases. The ubiquitin conjugation has been implicated in a variety of cellular processes, including cell-cycle control, signal transduction, transcriptional regulation, and cell death (8, 9). Furthermore, the conjugation with ubiquitin also serves as a sorting signal that determines the destination of various proteins at the different subcellular organelles such as the plasma membrane, the trans-Golgi network, and the endosome (10). The conjugation of ubiquitin to substrate proteins requires at least three enzymes: the ubiquitin-activating enzyme (E1), a ubiquitin-conjugating enzyme (E2), and a ubiquitin ligase (E3). The RING-H2 finger is a zinc binding domain with an octet of cysteines and histidines with a defined space representing the largest class of ubiquitin ligases to date. For instance, mammalian genomes encode hundreds of RING finger proteins, and it has not yet been clear whether all of these proteins have E3 activity or not (11). In this regard, a number of molecules are waiting for characterization that may help us to understand how the intracellular protein levels are controlled. Despite the recent investigation of the Class C VPS in the membrane traffic of the yeast and mammals, the molecular mechanisms remain undefined. In this report, we demonstrate that hVPS18 is a genuine ubiquitin ligase E3 and search in the rat brain for interacting molecules with hVPS18 using the yeast two-hybrid screen. Here we identified SNK as one of the candidate substrates of the ubiquitin ligase activity of hVPS18.

MATERIALS AND METHODS

Yeast Two-hybrid Screen and cDNA Cloning—For the yeast two-hybrid screen, the yeast strain AH109 was transformed sequentially with pGBKT7-hVPS18, as a bait, and a cDNA library of the rat brain (BD Biosciences Clontech) using the lithium acetate method. We screened 2×10^6 transformants on the plate containing synthetic dropout medium lacking histidine, tryptophan, and leucine. Positive clones were selected on 5 mM 3-aminotriazole-containing medium lacking leucine, tryptophan, and histidine and verified with a filter assay for β-galactosidase activity. The prey plasmids were recovered and sequenced. The full-length SNK was isolated by reverse transcription-PCR from the rat brain cDNA. We assessed the interaction of hVPS18 and rat SNK in AH109 cells transformed sequentially with pGBKT7-hVPS18 (full-length or ΔRING) and pGADT7 containing SNK or clone #A12–1 by quantifying β-galactosidase activity.

* This work was funded by Ministry of Health, Labor, and Welfare, Japan and by a grant-in-aid for Scientific Research from the Ministry of Education, Science, Sports and Culture of Japan. The costs of publication of this article were defrayed in part by the payment of page charges. This article must therefore be hereby marked "*advertisement*" in accordance with 18 U.S.C. Section 1734 solely to indicate this fact.

[1] To whom correspondence should be addressed. Tel.: 81-423-41-2711; Fax: 81-423-46-1751; E-mail: kohsaka@ncnp.go.jp.

[2] The abbreviations used are: Plk, polo-like kinase; VPS, vacuolar protein sorting; SNK, serum-inducible kinase; PBD, polo-box domain; E1, ubiquitin-activating enzyme; E2, ubiquitin-conjugating enzyme; E3, ubiquitin ligase; shRNA, short hairpin RNA; CMV, cytomegalovirus; HA, hemagglutinin; hVPS, human VPS; DMEM, Dulbecco's modified Eagle's medium; BrdU, bromodeoxyuridine; ERK, extracellular signal-regulated kinase; SPAR, spine-associated Rap guanosine triphosphatase (GTPase)-activating protein; NHS, *N*-hydroxysuccinimide.

Plasmid Construction—Full-length and various truncated SNK cDNAs were subcloned into the following vectors: the pGEX-4T2 (Amersham Biosciences) prokaryotic expression vector for the production of GST-tagged fusion proteins; the pCMV-HA, pCMV-FLAG, and pCMV-Myc mammalian expression vectors (BD Biosciences Clontech) for the production of HA-tagged, FLAG-tagged, and Myc-tagged fusion proteins. Myc-tagged and HA-tagged hVPSs (hVPS11, hVPS18, hVPS18ΔRING, hVPS16, and hVPS33a) mammalian expression vectors were prepared as described previously (6). The full-length hVPSs (hVPS11, hVPS18, and hVPS16) were subcloned into pFastBacHTb insect expression vector (Invitrogen) to generate His-tagged hVPSs.

Expression and Preparation of Recombinant Proteins—Ubiquitin-conjugating enzymes (E2s) were expressed in *E. coli* strain BL21-AI (Invitrogen) and lysed in a buffer containing phosphate-buffered saline, 1 mM phenylmethylsulfonyl fluoride, and Complete protease inhibitor mixture (Roche Molecular Biochemicals). The supernatant, after centrifugation at 14,000 × *g* for 10 min, was used for the ubiquitylation reaction. Full-length and various truncated mutants of GST-SNK were expressed in *E. coli* strain BL21-AI, and the recombinant proteins were purified using glutathione-Sepharose 4B beads (Amersham Biosciences) in phosphate-buffered saline, 1 mM phenylmethylsulfonyl fluoride, Complete protease inhibitor mixture. His-tagged hVPSs (hVPS11, hVPS18, and hVPS16) were expressed in Sf9 insect cells using baculovirus protein expression system (Invitrogen), and the recombinant proteins were purified by using ProBond metal affinity beads (Invitrogen) in a buffer containing 50 mM Tris-HCl, pH 7.4, 3 mM $MgCl_2$, 0.1% Nonidet P-40, 1 mM phenylmethylsulfonyl fluoride, 200 mM NaCl.

Cell Culture and DNA Transfection—COS7, HeLa, and HEK293T cells were maintained in Dulbecco's modified Eagle's medium (DMEM) supplemented with 10% fetal bovine serum, 100 units/ml penicillin, and 100 μg/ml streptomycin in humidified incubators with 5% CO_2 at 37 °C. The cells were transfected with various plasmids by FuGENE 6 reagent (Roche Molecular Biochemicals) according to the manufacturer's instructions.

Antibodies—His-tagged full-length rat SNK was expressed in Sf9 cells. The protein was purified by ProBond metal affinity resin and used as immunogens in Wistar rats. The affinity purification using His-SNK coupled to a HiTrap NHS-activated column (Amersham Biosciences) was performed according to the manufacturer's instruction. The rabbit anti-SNK polyclonal antibody was kindly provided by Dr. M. H. Sheng. Anti-hVPS antibodies (hVPS11, hVPS16, and hVPS18) were prepared as described previously (6). Other antibodies used were as follows: mouse monoclonal anti-Myc antibody (9E10, Roche Molecular Biochemicals), rat monoclonal anti-HA antibody (3F10, Roche Molecular Biochemicals), mouse monoclonal anti-FLAG (M2)-agarose (Sigma), rabbit polyclonal anti-ubiquitin antibody (Sigma), and mouse monoclonal anti-α-tubulin antibody (B-5-1-2, Sigma).

Immunoprecipitation—For immunoprecipitation, the cells were lysed in modified radioimmune precipitation assay buffer (50 mM Tris, pH 7.6, 250 mM NaCl, 1% Triton X-100, 3 mM EDTA) supplemented with Complete protease inhibitor mixture. Total cell lysates were centrifuged at 10,000 × *g* for 10 min, and the protein concentration of the supernatants was determined. Identical amounts of the protein from each sample were precleared by incubation with protein A/G Sepharose 4 fast flow (Amersham Biosciences) for 30 min at 4 °C. After the removal of protein A/G-Sepharose by brief centrifugation, the solution was incubated with 2 μg of monoclonal anti-Myc antibody, monoclonal anti-HA antibody, or control IgGs at 4 °C overnight. Immunoprecipitation of the antigen-antibody complex was accomplished by adding 40 μl of protein A/G-Sepharose for 1 h at 4 °C. Sepharose-bound proteins were solubilized in 40 μl of SDS sample buffer. Samples were boiled and separated by SDS-PAGE, and Western blot analyses were performed.

In Vitro Pull-down Assay—Full-length and various truncated mutants of GST-SNK were immobilized on glutathione-Sepharose 4B beads and equilibrated with wash buffer (50 mM Tris-HCl, pH 7.4, 150 mM NaCl, 0.1% Triton X-100, 3 mM $MgCl_2$, 0.1 mM phenylmethylsulfonyl fluoride) for three times. The resin was incubated with His-tagged hVPSs at 25 °C for 30 min and washed with the wash buffer for three times. The resin was subjected to SDS-PAGE, and Western blot analyses were performed by either anti-hVPS18 antibody, anti-hVPS11 antibody, or anti-hVPS16 antibody.

In Vivo and in Vitro Ubiquitylation Assay—Myc-tagged hVPS18, hVPS11, hVPS16, FLAG-tagged SNK, and HA-tagged ubiquitin were co-transfected to COS7 cells using FuGENE 6. Transfected cells were treated with 30 μM MG132 for 3 h at 16 h post-transfection. Immunoprecipitation was performed by using anti-FLAG (M2)-agarose, and conjugated HA-ubiquitin was detected by Western blot analyses using anti-HA antibody.

An *in vitro* ubiquitylation assay was performed as described previously (12). GST-SNK full-length was mixed with yeast E1 (500 ng, Boston Biochem), E2-enzyme mixture (Boston Biochem), or UbcH4, ubiquitin (10 μg, Boston Biochem) and His-hVPS18. The mixture was incubated at 25 °C for 30 min in the presence of 50 mM Tris-HCl, pH 7.4, 5 mM $MgCl_2$, 2 mM dithiothreitol, and 2 mM ATP in a 50-μl volume. After incubation, the mixture was subjected to SDS-PAGE and detected by Western blot analyses using anti-GST antibody, anti-ubiquitin antibody, or anti-hVPS18 antibody.

Establishment of HeLa Cell Lines Up-regulates/Down-regulates hVPS18 by Lentivirus Vector—The lentivirus containing full-length of hVPS18 or short hairpin RNA (shRNA) interference was raised by the method previously described (13). Briefly, synthetic oligonucleotides (top-strand: 5′-GATCCCCAGGTGTCCATCTTCGCAAAGCGTGTGCTGTCCGCTTTGTGAAGATGGGCACTTTTTTTGGAAAT-3′; bottom-strand: 5′-CTAGATTTCCAAAAAAAGTGCCCATCTTCACAAAGCGGACAGCACACGCTTTGCGAAGATGGACACCTGGG-3′; underline, loop sequence) were annealed and ligated into the BglII-XbaI site of pENTR4-H1. The full length of hVPS18 cDNA was ligated into the EcoRI-XhoI site of pENTR3C. Then either pENTR4-H1-hVPS18-shRNA or pENTR3C/hVPS18 was incubated with pLent6/V5 DEST (Invitrogen) in the presence of Gateway LR Clonase (Invitrogen) for plasmid recombination. To obtain recombinant lentivirus, the Clonase-recombinated plasmid was co-transfected with packaging construct (pCAG-HIVgp), and vesicular stomatitis virus G glycoprotein-expressing, Rev-expressing construct (pCMV-VSV-G-RSV-Rev) to HEK293T cells. The titer of virus was determined by measuring the amount of human immunodeficiency virus, type 1 p24 gag antigen using an enzyme-linked immunosorbent assay kit (PerkinElmer Life Sciences). The recombinant lentivirus (titer: 5 × 10^7 IU/ml) was infected to HeLa cells with 10 μg/ml Blasticidin S (Invitrogen) to select the virus-infected cells. The Blasticidin S-resistant colony was identified and expanded to establish the HeLa cell lines that constitutively overexpress hVPS18 (HeLa-hVPS18(OE)) or constitutively knock-down hVPS18 by shRNA interference (HeLa-hVPS18(shRNA)). To confirm the expression level of hVPS18 and SNK in the established HeLa cell lines, Western blot analyses and immunocytochemistry were performed as previously described (6).

[^{35}S]Methionine and [^{35}S]Cysteine Pulse-chase Analysis—Three lines of HeLa cells (Control, hVPS18(OE), and hVPS18(shRNA)) were subjected to the *in vivo* pulse-chase analyses using [^{35}S]methionine/

[^{35}S]cysteine. Each cell was washed with phosphate-buffered saline three times and incubated for 1 h with Met(−)/Cys(−)-DMEM without serum. The medium was then replaced with Met(−)/Cys(−)-DMEM containing 1 mCi of [^{35}S]Met/[^{35}S]Cys Express Protein Labeling Mixture (Amersham Biosciences) and 10% fetal bovine serum. After incubation for 2 h, the medium was replaced with non-radioactive DMEM complete medium. Cells were then incubated for indicated chase time and harvested. Cells were lysed and immunoprecipitated, using anti-SNK antibody and protein A/G-Sepharose 4 fast flow. Immunoprecipitates were subjected to SDS-PAGE and detected by BAS5000 image analyzer (FUJI Film).

Flow Cytometric Analysis—Cell cycle of HeLa cells was synchronized and released from G_1/S arrest. Briefly, the cells were treated with 3 μg/ml aphidicolin and serum starvation for 14 h. Then, the cells were stimulated to progress the cell cycle by with 10% serum in the absence of aphidicolin for the indicated times. Prior to each harvest, the cells were labeled for 30 min in the presence of BrdUrd at the concentration of 10 μM. For immunostaining of BrdUrd-incorporated DNA, cells were treated as recommended by the manufacturer (BrdU Flow Kit, BD Biosciences). Subsequently, cells were stained with propidium iodide and subjected to fluorescence-activated cell sorting analyses based on DNA content. The each sample (1×10^6 cells) was analyzed by the cell-cycle distribution using FACStar cell sorter (BD Bioscience).

RESULTS

RING-H2 Domain of hVPS18 Has a Ubiquitin Ligase Activity—It has been shown that hVPS18, a member of Class C VPS protein, has a RING-H2 finger domain in its C-terminal region (6). To examine whether hVPS18 has a ubiquitin ligase activity, we performed *in vitro* ubiquitylation assay using an *E. coli* lysate as an anonymous substrate. Because Nedd4 has a HECT (homologous to E6-associated protein carboxy terminus) type ubiquitin ligase activity, we used Nedd4 as a positive control of E3 activity (Fig. 1*A*, *lane 7*). As shown in Fig. 1*A*, the ubiquitylated proteins were detected in the presence of E1, E2-enzyme mixture, hVPS18, ubiquitin (Fig. 1*A*, *lane 6*) but not detected in the absence of either E1, E2, hVPS18, or *E. coli* lysate (Fig. 1*A*, *lanes 1–5*). Therefore, hVPS18 has a ubiquitin ligase activity using bacterial proteins as substrates. In a series of ubiquitylation pathways, it is required for the specific interaction between E3, E2, and substrate, to transfer ubiquitins to a target substrate. To examine the selectivity and the specificity of E2 enzymes for hVPS18, we performed *in vitro* ubiquitylation assay using various E2 enzymes. As shown in Fig. 1*B*, hVPS18 has a preference for UbcH4 (Fig. 1*B*, *lane 5*). Moreover, we examine whether RING-H2 domain of hVPS18 is responsible for ubiquitin ligase activity. As shown in Fig. 1*C*, hVPS18ΔRING does not have ubiquitin ligase activity *in vitro* (Fig. 1*C*, *lane 3*), suggesting that VPS18 functions as a ubiquitin ligase depending on its RING-H2 domain.

Identification of SNK That Interacts with hVPS18—To explore the interacting proteins with hVPS18, we screened the rat brain cDNA library by yeast two-hybrid using the full-length human hVPS18 cDNA as a bait. From the screening of 2×10^6 clones, we obtained some rat clones encoding the homologues of hVPS11, hVPS16, and hVPS33a (data not shown), that have been shown to constitute a hetero-oligomeric complex with hVPS18, confirming the validity of this screen. Four of the positive clones, two identical clones (*clone #A12-1*, Fig. 2*A*) and two independents, have a sequence identity with the rat SNK cDNA (accession number: NM_031821), which was previously characterized as a new type of serine/threonine kinase highly induced in the presence of serum and stimuli that produce synaptic plasticity (14, 15). SNK is one of the Plks that associate with cell cycle (16–18). The full-length

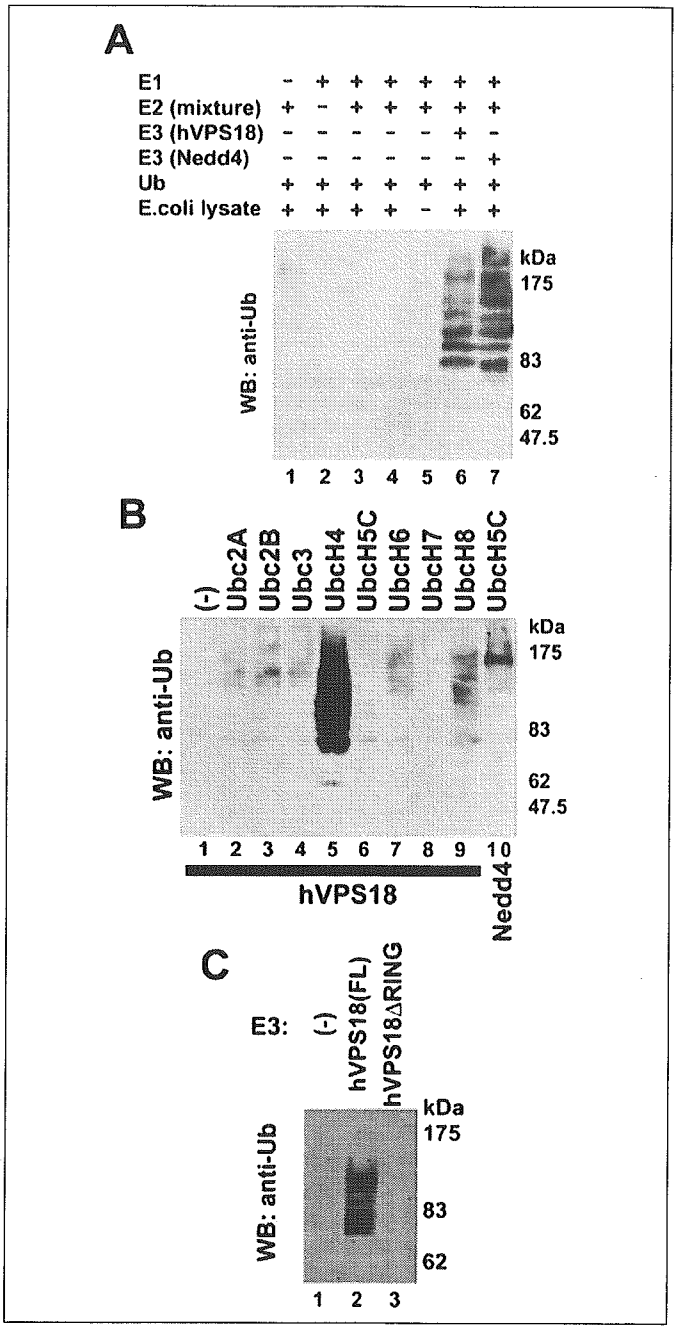

FIGURE 1. **hVPS18 is a RING-H2 type ubiquitin ligase.** *A*, the *in vitro* ubiquitylation reaction was performed in the presence or absence of purified His-hVPS18 or Nedd4, E1, E2-enzyme mixture, ubiquitin, and *E. coli* lysate as substrate at 25 °C for 30 min. After the reaction, the proteins were resolved by SDS-PAGE and detected by Western blot analyses using anti-ubiquitin antibody. The ubiquitylated proteins were detected in *lanes 6* and *7*. *B*, to examine E2 selectivity for hVPS18, the *in vitro* ubiquitylation reaction was performed. The ubiquitylation of proteins by hVPS18 was selectively mediated by UbcH4. *C*, the *in vitro* ubiquitylation reaction was performed in the presence of His-hVPS18 or His-hVPS18ΔRING. ΔRING, C-terminal deletion of RING-H2 of hVPS18. The RING-H2 domain is necessary for the ubiquitylation by hVPS18.

SNK cDNA revealed that SNK is a 682-amino acid protein with calculated molecular mass of 77.8 kDa, containing kinase domain at the N-terminal regions and polo-box domain (PBD) at the C-terminal regions (14, 19).

We further confirmed the interaction of hVPS18 and SNK using the two-hybrid assays. Results of β-galactosidase color reaction were summarized in Fig. 2*B*. The clone A12-1 and full-length SNK bind to both

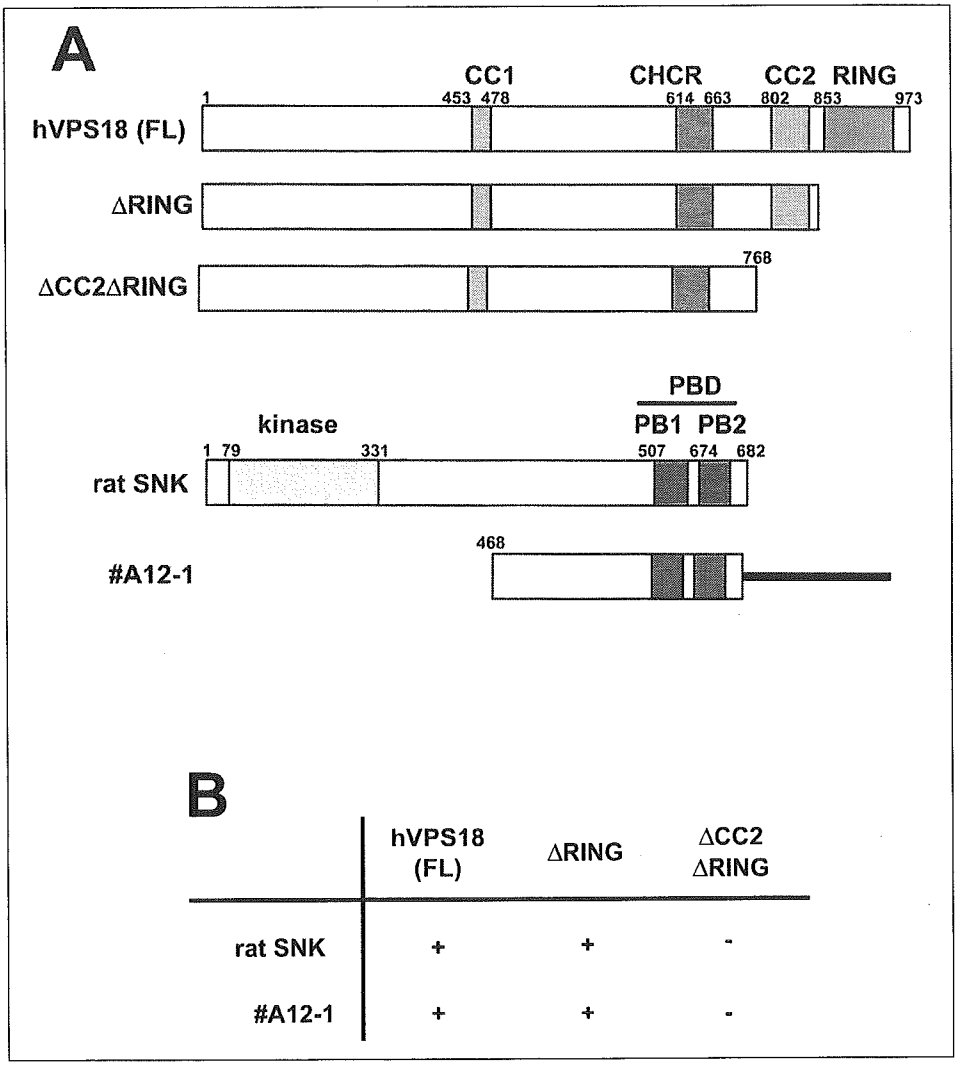

FIGURE 2. **Interaction of hVPS18 and SNK in yeast cells.** *A*, schematic representation of hVPS18 (full-length, ΔRING, and ΔCC2ΔRING), and SNK (full-length and A12-1). The clone *#A12-1* is a partial fragment of SNK isolated from the yeast two-hybrid screen. *ΔCC2*, C-terminal deletion at the second coiled-coil region of hVPS18. *B*, the interaction of hVPS18 and SNK was confirmed by β-galactosidase assay in yeast cells. The interaction between hVPS18 and SNK was abolished when the second coiled-coil region of hVPS18 was deleted. +, detectable by β-galactosidase activity; −, not detectable. *FL*, full-length; *CC*, coiled-coil; *CHCR*, chattering heavy chain repeat; *PBD*, polo-box domain; *PB*, polo-box.

the full-length hVPS18 (FL) and hVPS18 lacking RING-H2 domain (ΔRING), but not to hVPS18 lacking the C-terminal coiled-coil domain and RING-H2 domain (ΔCC2ΔRING). This suggests that hVPS18 interacts with SNK through the second coiled-coil domain.

hVPS18 Interacts with SNK in Vitro and in Vivo—To answer the question whether the full-length SNK interacts with hVPS18, we performed immunoprecipitation assays. HEK293T cells were transfected with Myc-SNK and HA-tagged hVPS11, hVPS18, hVPS16, and hVPS33a, respectively. As shown in Fig. 3*A*, SNK was efficiently co-immunoprecipitated with hVPS18 and the other Class C VPS. Please note that the interaction between SNK and hVPS18 is strongest among other members of Class C VPS complex. To further confirm the association of SNK and the Class C VPS *in vitro*, we performed an *in vitro* pull-down assay. The bacterial expressed GST-SNK was immobilized on glutathione beads, and insect-expressed His-tagged hVPS11, hVPS18, and hVPS16 were loaded. As shown in Fig. 3*B* (*lanes 1–6*), in a good agreement with the data obtained in the yeast two-hybrid screen, GST-SNK preferentially interact with His-hVPS18. As shown in Fig. 3*B* (*lanes 7–12*), hVPS11 and hVPS16 were retained with GST-SNK in the presence of hVPS18. These results suggest that the interaction between SNK and other Class C VPS in co-immunoprecipitation assay is partly mediated by hVPS18, and all of the Class C VPS proteins may constitute a large hetero-oligomeric complex *in vivo* (6).

Because the highly conserved PBD plays an important role for the correct subcellular localization and molecular interaction, we performed *in vitro* pull-down assays using the bacterially expressed GST proteins fuse to the various deletion forms of SNK. As shown in Fig. 4, SNK full-length and deletion mutants containing PBD at the C-terminal regions, efficiently bind to hVPS18, indicated that the PBD of SNK is involved in protein-protein interaction consistent with previous report (20, 21).

VPS18 Ubiquitylates SNK in Vitro and in Vivo—To answer the question whether SNK is ubiquitylated by hVPS18, we performed ubiquitylation assays of SNK *in vivo* and *in vitro*. COS7 cells were co-transfected with FLAG-tagged SNK, and various combinations of Myc-tagged hVPS18, hVPS11, and hVPS16, in the presence or absence of HA-tagged ubiquitin. As shown in Fig. 5*A*, SNK was heavily conjugated with HA-ubiquitin in the cells overexpressing hVPS18 (Fig. 5*A*, *lane 3*). The faint smearing in *lanes 2*, *4*, and *5* suggests the possibility that SNK was ubiquitylated by endogenous VPS18 or other anonymous E3 of COS7 cells. It is necessary to observe the direct ubiquitylation of SNK by hVPS18 *in vitro*, we carried out ubiquitylation assays in which bacterially expressed GST-SNK proteins were incubated in the presence of E1, E2, His-hVPS18, ubiquitin, and ATP. As shown in Fig. 5*B*, SNK was ubiquitylated dependent on hVPS18, suggesting that SNK is one of the target substrates for hVPS18 E3 ubiquitin ligase.

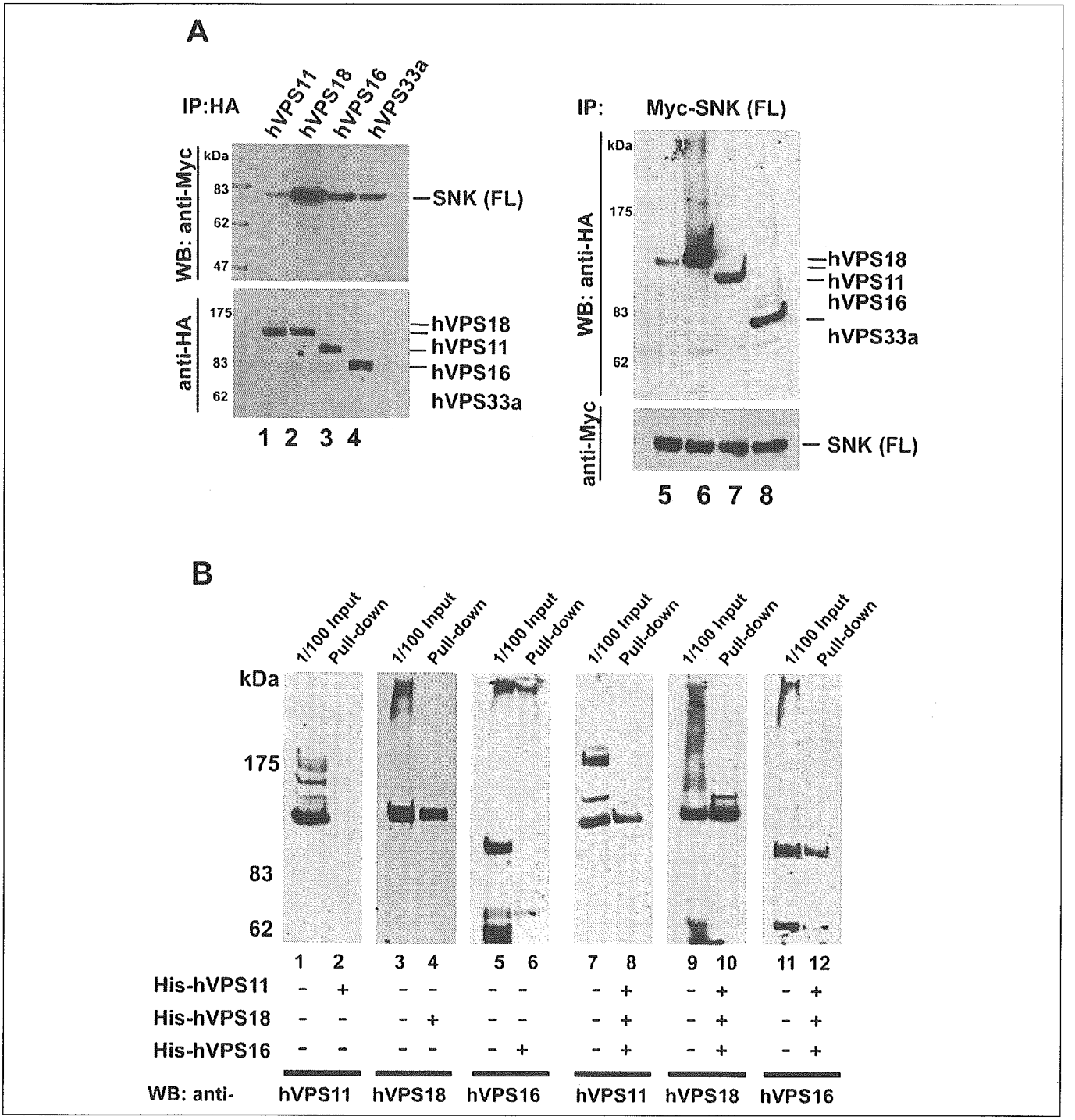

FIGURE 3. **Interaction of hVPS18 and SNK *in vivo* and *in vitro*.** *A* (*left*), HEK293T cells were co-transfected with Myc-SNK and either HA-tagged hVPS11, hVPS18, hVPS16, or hVPS33a, respectively. At 24 h post-transfection, whole cell lysates were immunoprecipitated using anti-HA antibody. Immunoprecipitates were resolved by SDS-PAGE and detected by Western blot analyses using anti-Myc antibody (*upper panel*). The membrane was then stripped and blotted with anti-HA antibody (*lower panel*). HA-hVPS18 strongly precipitated Myc-SNK (*lane 2*). *Right*, conversely, immunoprecipitation was performed using anti-Myc antibody, and the interacting molecules were detected by anti-HA antibody. *B*, GST-SNK was immobilized on glutathione-Sepharose 4B beads and incubated with His-tagged hVPS18, hVPS11, or/and hVPS16 at 25 °C for 30 min. The resin was washed and subjected to SDS-PAGE, and Western blot analyses were performed with indicated antibodies. His-hVPS18 interacted directly interacted with GST-SNK *in vitro*.

HeLa Cell Lines That Overexpress hVPS18 or Knockdown hVPS18—To characterize the physiological relation of SNK and hVPS18, we established HeLa cells that overexpress hVPS18 (HeLa-hVPS18(OE)) or shRNA interference of hVPS18 (HeLa-hVPS18(shRNA)) by lentivirus. After infection with the recombinant lentivirus, HeLa cells were treated with 10 μg/ml Blasticidin S, which is a selection antibiotic drug of the recombinant lentivirus infection. After 7–14 days of incubation with Blasticidin S, the resistant colony was isolated and expanded. To confirm the expression level of hVPS18 and SNK, Western blot analyses were performed. Compared with the control HeLa cell, the cells treated with shRNA interference lentivirus of hVPS18 show up-regulated expression of SNK. Conversely, the cells overexpressing hVPS18 show

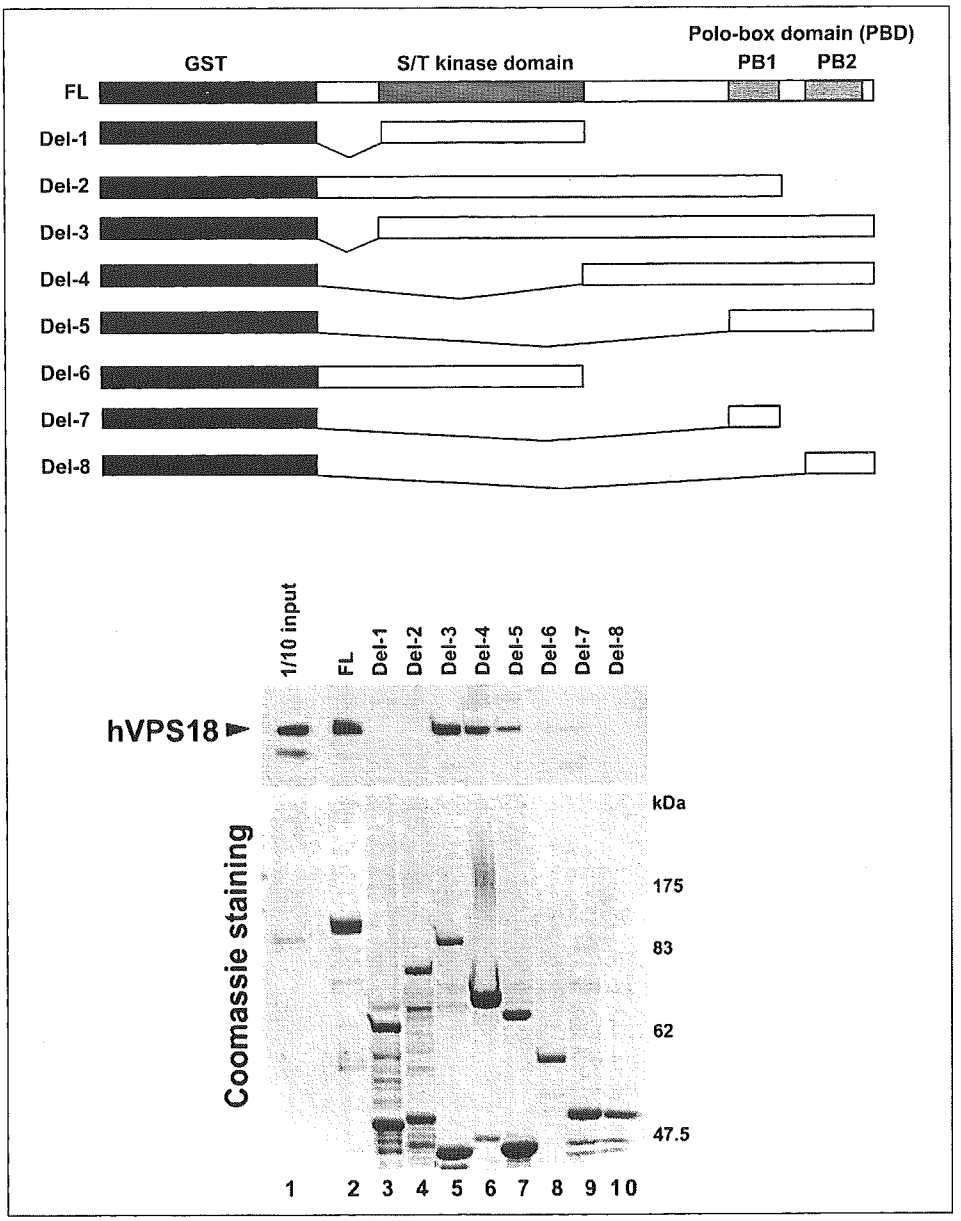

FIGURE 4. **Polo-box domain of SNK is necessary for binding with hVPS18 *in vitro*.** *Top*, schematic representation of SNK full-length and various deletion mutants used in the *in vitro* GST pull-down assays. *Bottom*, the *in vitro* pull-down assays of His-hVPS18 and either GST-SNK or various deletion mutants were performed. *Bottom*, GST-SNK proteins used in this study were shown as Coomassie Brilliant Blue (CBB) staining to confirm that the relatively equal amount of proteins was analyzed in each experiment.

down-regulated SNK (Fig. 6*A*). To define the subcellular localization of SNK and hVPS18, immunohistochemistry was performed using established HeLa cell lines as shown in Fig. 6*B*. Up-regulated expression of SNK was observed in the cells that knocked down hVPS18 by shRNA interference lentivirus, whereas down-regulated expression of SNK was observed in the cells overexpressing hVPS18. The reciprocal level of expression between hVPS18 and SNK strongly suggests the endogenous SNK expression is regulated, at least in part, by hVPS18.

To further analyze the role of hVPS18 in the SNK protein turnover, *in vivo* cell labeling by [^{35}S]Met/[^{35}S]Cys was performed. As shown in Fig. 7, the three lines of HeLa cells (control, hVPS18(OE), and hVPS18(shRNA)) were labeled and pulse-chased at five time points (0, 15, 30, 60, and 120 min). The total cell lysates were incubated with rat anti-SNK antibody, and the immunoreactive bands were resolved by SDS-PAGE. In general, polyubiquitylated proteins are promptly subjected to degradation by 26 S proteasome. In a good accordance with our results that SNK is ubiquitinylated, the level of SNK protein degraded quickly (half-life, 20 min, Fig. 7*B*) as shown in the control HeLa cells. When hVPS18 was overexpressed, the degradation of SNK protein was enhanced (half-life, 13.5 min, Fig. 7*B*). Conversely, the degradation of SNK protein was retarded in the HeLa cells knocked-down hVPS18 expression (half-life, 45 min, Fig. 7*B*). The degradation pattern was reproducible by using the independent antibody against SNK provided by Dr. M. Sheng (data not shown). These results suggest that the degradation of endogenous SNK in HeLa cells can be regulated by the level of hVPS18 expression.

Delayed Entry to S Phase When Overexpressed with hVPS18—Our hypothesis is that hVPS18 is involved in the degradation of SNK. It was previously reported that the kinase activity of SNK is required for centriole duplication close to the G_1 to S phase transition (16). Cultured SNK−/− embryonic fibroblasts showed delayed entry to S phase (18). We thus examined the cell-cycle progression of HeLa cells overexpressing hVPS18. Although the profile of cell cycle between control HeLa cells and hVPS18 overexpressing HeLa cells was almost similar, the proportion of cells to S phase after 20 h was significantly lower than the control HeLa cells (Fig. 8). These results are in good accordance with the

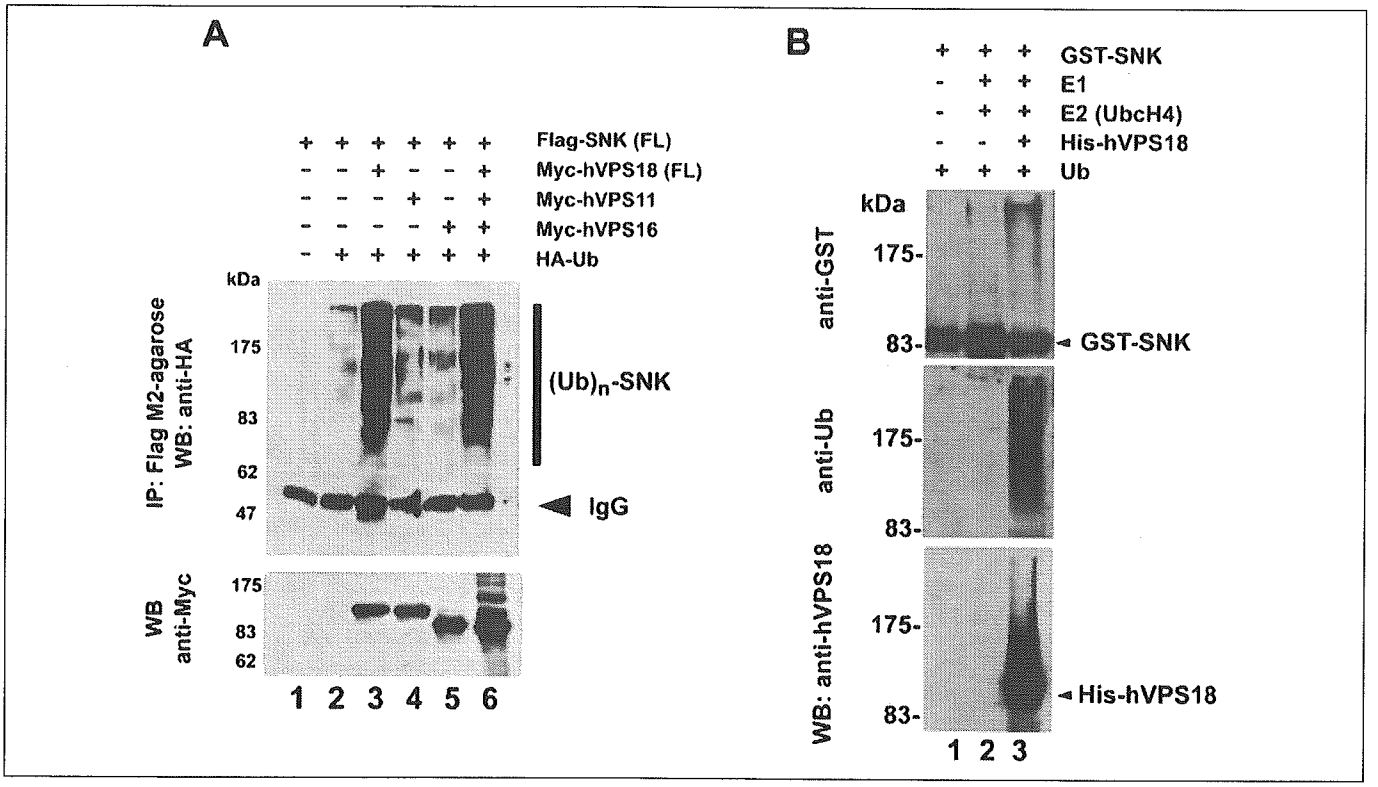

FIGURE 5. **hVPS18 but not other Class C VPS proteins promotes ubiquitylation of SNK.** *A*, ubiquitylation of SNK by Class C VPS proteins in transfected HEK293T cells. HEK293T cells were co-transfected with FLAG-SNK and either pCMV-Myc vector, Myc-tagged hVPS11, hVPS18, hVPS16, hVPS33a, and HA-ubiquitin. At 16 h post-transfection, the cells were further incubated for 3 h with the protease inhibitor, MG132 (30 μM). Whole cell lysates were immunoprecipitated using anti-FLAG (M2)-agarose. Immunoprecipitates were resolved by SDS-PAGE and detected by Western blot analyses using anti-HA. *B*, the *in vitro* ubiquitylation reaction was performed in the presence of GST-SNK, E1, UbcH4, ubiquitin, and His-hVPS18 at 25 °C for 30 min. The proteins in the reaction were resolved by SDS-PAGE and detected by Western blot analyses using anti-GST antibody (*top panel*), anti-ubiquitin antibody (*middle panel*), or anti-hVPS18 antibody (*bottom panel*).

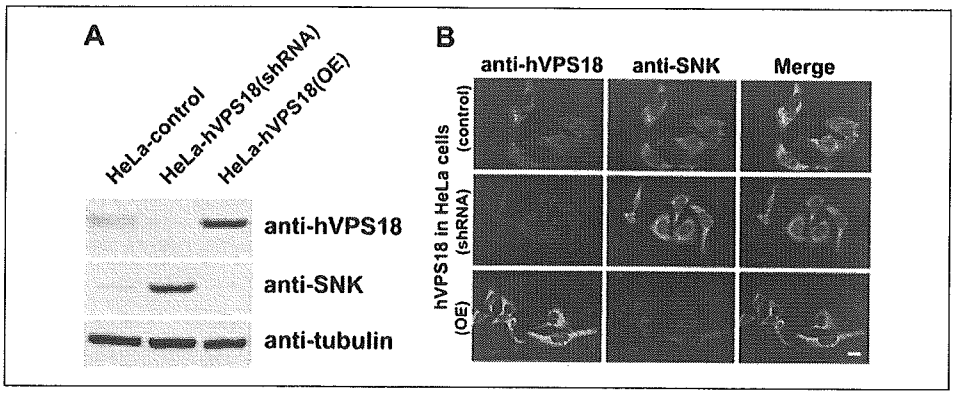

FIGURE 6. **Isolation of HeLa cells knocked-down hVPS18 (*shRNA*) expression or overexpressed-hVPS18 (*OE*) expression by lentivirus vector.** *A*, total cell lysate (30 μg) was resolved in SDS-PAGE and analyzed by Western blot analyses using indicated antibodies. Single colony HeLa cells was isolated and expanded in the presence of Blasticidin S (10 μg/ml) that is used for selection of lentivirus-infected cells. HeLa cells isolated after lentivirus of knocked-down construct of hVPS18 showed up-regulated expression of SNK. Meanwhile, HeLa cells isolated after lentivirus construct of full-length hVPS18; HeLa-hVPS18 (*OE*) showed down-regulated expression of SNK. Western blot analyses using anti-α-tubulin suggested that equal amounts of total lysate were loaded in each lane. *B*, immunocytochemistry was performed for HeLa cell to compare intracellular expression of hVPS18 and SNK. In the same scanning condition using confocal microscope, three HeLa cell lines (control, hVPS18(shRNA), and hVPS18(OE)) were analyzed using rabbit anti-hVPS18 antibody and rat anti-SNK visualized by fluorescent labeled secondary antibody. Consistent with Western blot analyses, SNK expression was regulated by the expression level of hVPS18. *Bar*, 20 μm.

null mutant analyses and suggest that the expression level of hVPS18 may regulate the SNK protein level *in vivo* (18).

DISCUSSION

The main findings of this study are that hVPS18 acts as a genuine ubiquitin ligase to induce the ubiquitylation and degradation of SNK using *in vitro* and *in vivo* experiments. The turnover of SNK protein was shortened by the overexpression of hVPS18, meanwhile the turnover was retarded by the shRNA interference of hVPS18. It suggests that the protein level of SNK is regulated by hVPS18. In HeLa cells overexpressing hVPS18, the delayed entry to S phase was observed during the cell-cycle progression. The targeted protein degradation has been increasingly understood to be a general mechanism by which cells properly regulate the intracellular protein levels. In eukaryotic cells, lysosomes/vacuoles are important organelles for the protein degradation. The Class C VPS complex has been intensively characterized as the mole-

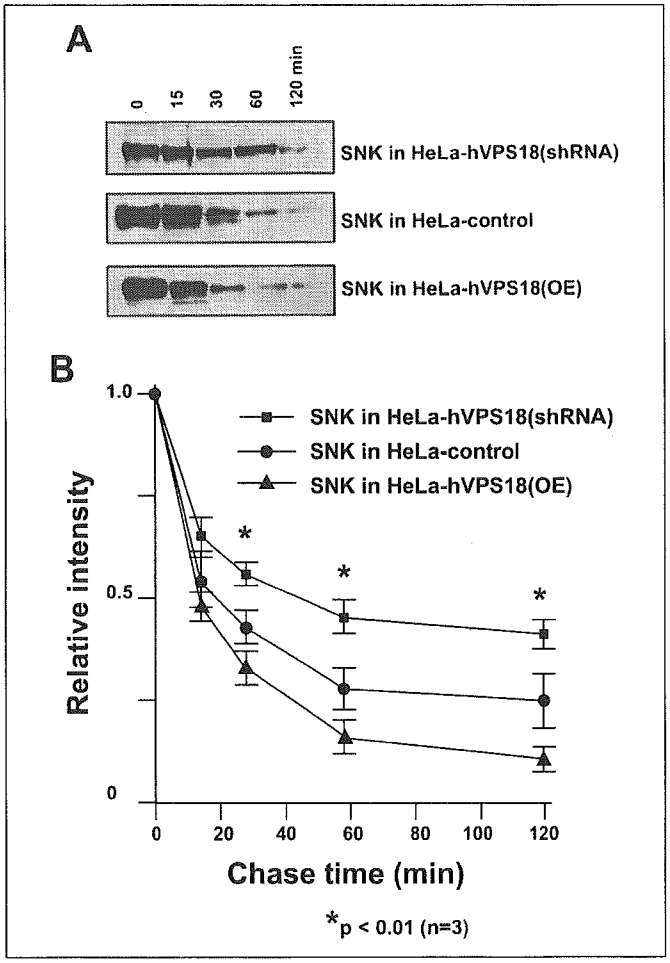

FIGURE 7. **Expression level of hVPS18 regulates intracellular SNK turnover.** *A*, representative results of film autoradiography. HeLa cells were radiolabeled for 1 h with DMEM medium containing [^{35}S]Met/Cys. The cells were chased for an indicated time after replacing with non-radioactive DMEM complete medium. The ^{35}S-labeled SNK was immunoprecipitated using rat anti-SNK antibody, resolved by SDS-PAGE, and autoradiography. *B*, the radioactive intensity of SNK was quantified using BAS5000, statistically analyzed (Student's *t*), and plotted for the relative amount of remaining SNK. Data are shown as mean ± S.E. (*error bar*) of the results from three independent experiments. *, $p < 0.01$ for each HeLa cell line.

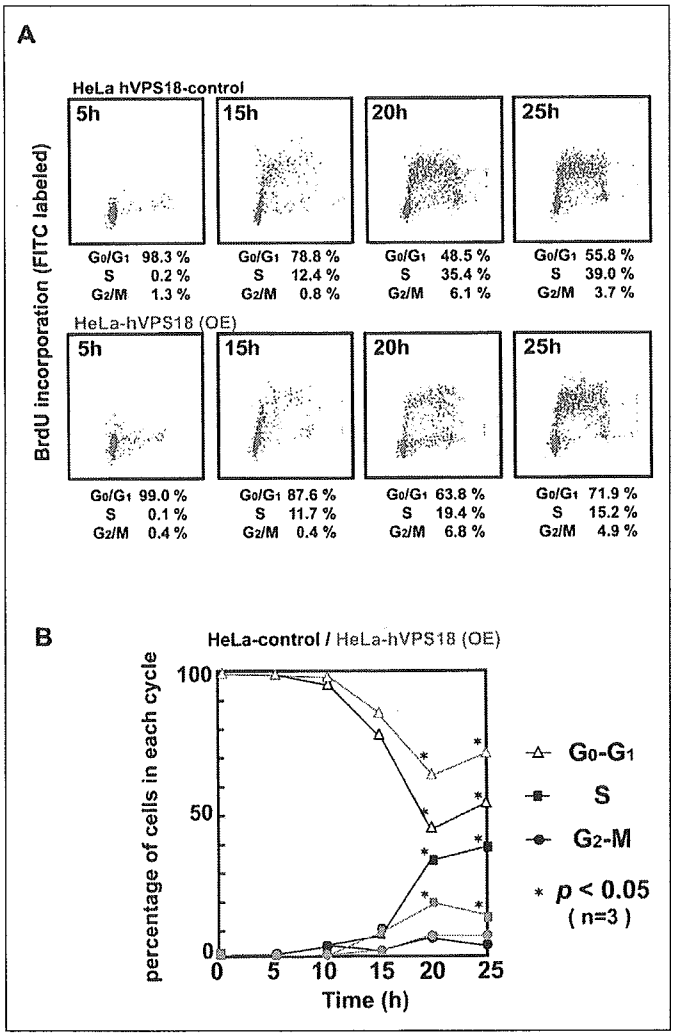

FIGURE 8. **Cell-cycle analyses by fluorescence-activated cell sorting.** *A*, representative result of cell-cycle profiles between the control HeLa cells (*HeLa-control*) and HeLa cells overexpressing hVPS18 (*HeLa-hVPS18 (OE)*). The cell cycle was synchronized by 14-h treatment of aphidicolin and serum starvation. The medium was changed and incubated to precede the cell cycle. The cells were labeled with BrdUrd for 30 min before harvesting, stained with anti-BrdUrd antibody and propidium iodide, and subjected to the flow cytometry. *B*, the percentages of cells in G_0-G_1, S, and G_2-M phase were *dotted*. The population of cells in S phase was smaller in the HeLa-hVPS18(OE) compared with the HeLa-control cells.

cules mediating the vesicle transport between late endosomes and lysosomes (6). Overexpression of VPS18 elicited abnormal perinuclear aggregation of late endosomes and lysosomes (22). Knockdown of VPS18 by RNA interference resulted in dispersion of these organelles throughout the cell periphery (23). Taken together with our current results that hVPS18 functions as ubiquitin ligase, it is possible to propose an overlapped mechanism of protein degradations between endosome/lysosome and ubiquitin-proteasome pathways through hVPS18.

hVPS18 contains several domains that are conserved in multiple species; a putative clathrin heavy chain repeat and coiled-coil domain that may mediate a protein-protein interaction, and C-terminal RING-H2 finger motif (6). The RING-H2 finger is a cysteine-rich, zinc-binding domain that is involved in diverse cellular processes, including transcriptional regulation, RNA transport, signal transduction, and membrane trafficking (9, 11). There are several lines of evidence showing that RING-H2 finger protein may function as a ubiquitin ligase. RING-H2 finger governs the transfer of ubiquitin from E2 to the protein substrate. From our *in vitro* experiments using anonymous substrates of *E. coli*, hVPS18 efficiently transferred ubiquitins from UbcH4. Because the recombinant hVPS18 devoid of RING-H2 did not show any E3 activity, the E3 activity of hVPS18 is dependent on its RING-H2 domain. In this report, we identified SNK as one of the target substrates for hVPS18 by the yeast two-hybrid screen. SNK was originally identified as an immediate-early transcript in NIH3T3 cells (14). The deduced amino acid sequences revealed that SNK is a member of Plks that are a family of serine/threonine kinases closely related to polo of *Drosophila* (24). Plks have been identified in evolutionarily diversified eukaryotes, and they share a conserved N-terminal kinase domain and a homologous non-catalytic C terminus. A domain of ~30 amino acid residues is highly conserved among these kinases and thus denoted as the polo-box domain (PBD) (19). One of the functions of PBD was described as a phosphoserine or phosphothreonine binding domain that mediates the targeting of Plks to the subcellular structures such as centrosomes (20, 25, 26). Previously, it was reported that endogenous SNK expression was regulated by the post-transcriptional level by showing the short half-life of ~15 min (17). Such a short half-life is reasonable from our results that SNK was ubiquitylated and degraded by ubiquitin-protea-